Review

Kyuho Kim, Kunwoo Park, Hyungchul Park, Sunkyu Yu, Namkyoo Park* and Xianji Piao*

Programmable photonic unitary circuits for light computing

Abstract: Unitarity serves as a fundamental concept for characterizing linear and conservative wave phenomena in both classical and quantum systems. Developing platforms that perform unitary operations on light waves in a universal and programmable manner enables the emulation of complex light–matter interactions and the execution of general-purpose functionalities for wave manipulations, photonic computing, and quantum circuits. Recently, numerous approaches to implementing programmable photonic unitary circuits have been proposed and demonstrated, each employing different design strategies that distinctly impact overall device performance. Here, we review foundational design principles and recent achievements in the implementation of programmable photonic unitary circuits, with a particular focus on integrated photonic platforms. We classify the design strategies based on the dimensionality of nontrivial unit operations in their building blocks: lower-dimensional unitary units, such as SU(2) operations, and higher-dimensional ones, such as Fourier transforms. In each category, recent efforts to leverage alternative physical axes, such as the temporal and frequency domains, to address scalability challenges are also reviewed. We discuss the underlying concepts, design procedures, and trade-offs of each design strategy, especially in relation to light-based computing.

Kyuho Kim and Kunwoo Park contributed equally to this work.

*Corresponding authors: Namkyoo Park, Photonic Systems Laboratory, Department of Electrical and Computer Engineering, Seoul National University, Seoul 08826, Korea, E-mail: nkpark@snu.ac.kr; and **Xianji Piao**, Wave Engineering Laboratory, School of Electrical and Computer Engineering, University of Seoul, Seoul 02504, Korea, E-mail: piao@uos.ac.kr. https://orcid.org/0000-0003-0865-2903
Kyuho Kim, **Kunwoo Park**, **Hyungchul Park and Sunkyu Yu**, Intelligent Wave Systems Laboratory, Department of Electrical and Computer Engineering, Seoul National University, Seoul 08826, Korea, E-mail: sunkyu.yu@snu.ac.kr (S. Yu). https://orcid.org/0000-0001-8667-6404 (S. Yu)

Keywords: unitary operation; photonic circuit; programmable photonics; photonic computing; universal unitary

1 Introduction

One of the fundamental postulates in elaborating traditional quantum theory is to assume an isolated system – one that neither exchanges energy nor matters with its environment [1]. This assumption allows the description of quantum systems using Hermitian Hamiltonians, which accompany mathematically well-established structures: real eigenspectra and orthonormal sets of eigenmodes. According to Stone's theorem [2], the temporal evolutions of quantum states are determined by the corresponding unitary propagators of Hamiltonians. Therefore, characterizing the unitary operations obtained from a quantum system directly corresponds to the complete description of the system as a solvable initial value problem, at least in the conservative regime of quantum physics. In this respect, the core operation principles of quantum computations, such as the gate operations and their circuit assemblies, are also developed under unitarity [3].

As a statistical average of quantum electrodynamics, classical optics often adopts the same assumption by neglecting material, structural, and radiation losses of optical systems [4]. Despite the lack of wavefunctions for photons [5], this radical approximation unveils the correspondence between classical wave equations and the Schrödinger equation, which has been the foundation of the analogy between classical and quantum wave phenomena [6], [7]. As a result, many classical optical phenomena can also be well described through unitary operations with sufficiently high accuracy. Inversely, achieving unitary operations through tailored optical systems allows not only the modelling of classical and quantum phenomena [8]–[13], but also the realization of conservative optical functionalities, such as light flow manipulation [14], modal engineering [15], [16], visual perception [17], and optical energy concentration [18].

Recently, light-based computing, especially in terms of data-driven [19]–[22] and quantum [23], [24] computations,

has attracted substantial attention to exploit the unique advantages of signal processing using photons – ultrahigh speed, low energy dissipation, and stable quantum states. These next-generation computing systems have sparked a surge of interest in realizing programmable and universal unitary operations in photonic platforms, which are essential ingredients for trainable photonic deep learning and general-purpose quantum computation. Among various optical platforms, such unitary operations are well developed mostly in photonic integrated circuits [25]–[27] in order to utilize their small footprint, stable light manipulation, and the elementwise modulation essential for reconfigurability. The rapid development of the field in terms of design [28]–[30] and fabrication [31]–[33] also supports the high-fidelity realization of universal unitaries for computing applications.

In this review, we investigate and classify various approaches of constructing programmable and universal forms of N-dimensional unitary operations in integrated photonics, focusing on their design philosophy, theoretical and numerical assessments, and pros and cons in terms of application devices. In Section 2, we briefly review the universality of unitary operations in photonics and its connection to light-based computing. In Sections 3 and 4, we exhibit the classification of design strategies according to the dimensionality of nontrivial unit operations, discussing

the building blocks of each method, their implementation platforms, and the following performances, such as fidelity and scalability. In the last section, we summarize the review and provide an outlook on the potential research topics, focusing on remaining challenges in scalability and fidelity.

2 Unitary operations in photonics

Unitary operations of light waves are observed ubiquitously in various photonic platforms. The most straightforward example is an isolated system composed of optical elements, such as coupled waveguides [8] and resonators [34], photonic crystals [18], and dielectric metamaterials [35] (Figure 1a). When the interactions with its environment, such as radiative or material loss, amplification, and dynamical changes of system parameters, are negligible within the temporal range of interest, the system can be well modelled with the following Schrödinger-form equation using the Hermitian Hamiltonian H:

$$i\frac{\mathrm{d}}{\mathrm{d}\xi}|\Psi\rangle = H|\Psi\rangle, \tag{1}$$

where $|\Psi\rangle$ is the state of light inside the system, and ξ depicts the evolution variable that can denote a spatial or temporal axis. The evolution of an optical state within the system is determined by the relation, $|\Psi(\xi)\rangle =$
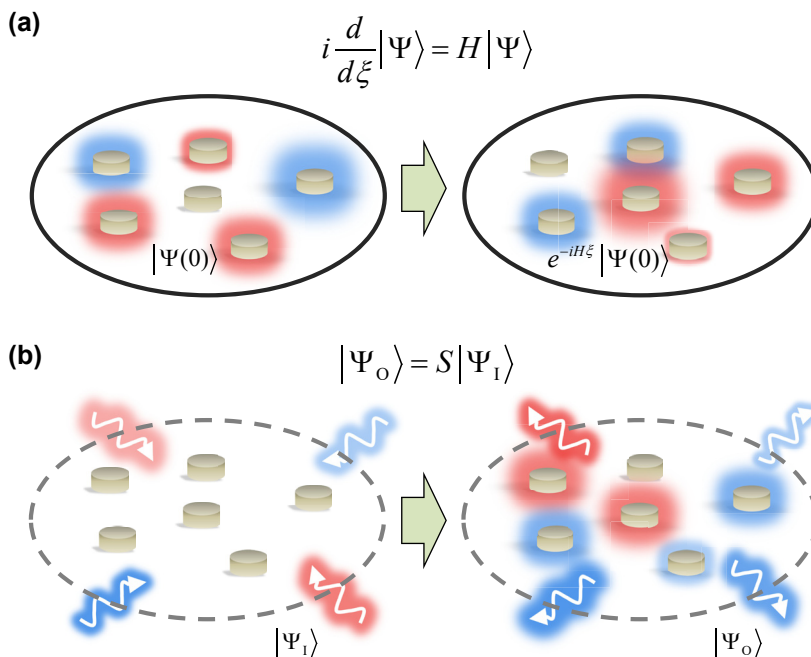

Figure 1: Unitary operations in photonics. (a) Schematic for unitary operations in isolated systems. The initial state $|\Psi(0)\rangle$ is evolved to be $|\Psi(\xi)\rangle = \exp(-iH\xi)|\Psi(0)\rangle$, which is governed by the unitary propagator $\exp(-iH\xi)$ from the Hermitian Hamiltonian H. (b) Schematic for unitary operations in open systems. The input state $|\Psi_I\rangle$ evolves to $|\Psi_O\rangle = S|\Psi_I\rangle$, which is governed by the unitary scattering operator S. The solid and dashed circles denote the isolated and open system boundaries, respectively. Disks represent optical materials inside the systems. Red and blue colors denote optical fields.

$\exp(-iH\xi)|\Psi(0)\rangle$, where the propagator $\exp(-iH\xi)$ is unitary due to the Hermiticity of H [2]. For example, light flows inside coupled waveguides or resonators are fully described by the unitary operator $\exp(-iH\xi)$ for any forms of the initial state $|\Psi(0)\rangle$. Notably, the platforms manipulating H in a reconfigurable manner have been widely applied to mimic the state evolutions in the corresponding quantum systems [10]–[13], [36].

On the other hand, unitary operations also play a critical role in open systems. Consider an open system in photonics (Figure 1b), which undergoes scattering [37] and diffraction [38]. When the system allows for incident and outgoing wave flows, while interactions with other physical domains – again, manifested as material gain and loss, or system dynamics – are negligible, light behaviors around the system are fully described by the scattering matrix:

$$|\Psi_O\rangle = S|\Psi_I\rangle, \tag{2}$$

where $|\Psi_I\rangle$ and $|\Psi_O\rangle$ denote the incident and scattering waves, respectively, of the same dimension. Due to energy conservation, the relationship $\langle\Psi_O|\Psi_O\rangle = \langle\Psi_I|S^\dagger S|\Psi_I\rangle = \langle\Psi_I|\Psi_I\rangle$ holds for arbitrary $|\Psi_I\rangle$, leading to $S^\dagger S = I$. Therefore, the scattering matrices S for open systems, satisfying $S^\dagger S = SS^\dagger = I$, correspond to unitary operations.

The above categorization of isolated and open systems is not a rigorous one but rather one of convenience. For example, when we consider recent interests on exploiting a temporal axis [39]–[44], the evolution along $\xi = t$ can be considered the scattering process with the scattering matrix $\exp(-iHt)$, where H describes the temporal variation of an optical potential. Similarly, the scattering matrix description with S can be understood as the energy exchange between eigenmodes when the entire space-time domain including the environment is considered an isolated system for light. Notably, as long as the system preserves energy of light waves, light behaviors in both isolated and open linear systems can be characterized by unitary operations.

Therefore, achieving high-dimensional, reconfigurable, and stable unitary operations of light through tailored photonic systems is a pivotal step toward advanced functionalities using light signals [25], [26]. For example, the recent surge of interest in photonic deep learning accelerators [45] has stimulated the efforts on achieving high-dimensional unitary operations for modelling weight matrices. When applying the singular value decomposition to an arbitrary weight matrix W, as $W = UDV^\dagger$, where U and V are unitary matrices and D is a diagonal matrix, realizing a universal and reconfigurable form of unitary matrices enables

trainable weight matrices for deep learning. The conservative nature of unitary operations has also attracted substantial attention for realizing unitary neural networks [46] to address the gradient explosion or vanishing problem during the learning process [47]–[49]. Another important application includes unit operations for linear optical quantum computing (LOQC) [23]. Because quantum computation generally exploits isolated systems, elementary gates and their circuit assemblies dictate the use of unitary optical elements. Therefore, the implementation of universal unitary operations is indispensable for reconfigurable and higher-dimensional photonic quantum computing [50]–[54]. In terms of classical light devices, reconfigurable diffractive and scattering platforms with unitary natures are also crucial for free-space data-driven computation [55], [56], and high-quality optical imaging, detection, and beam manipulations [57]–[60] from energy conservation. In these classical, quantum, and data-driven applications, we emphasize that the dimension of the obtained unitary matrix operations determines the ultimate information capacity supported by the system: the number of neurons in deep learning accelerators, the dimension of quantum gates for qudit operations, and the number of accessible channels in classical light devices.

In the following sections, we introduce various analytical and numerical strategies to realize high-dimensional ($N > 2$), universal, and reconfigurable U_N matrices for light waves. The methods are classified by two categories: the systematic assemblies of (i) lower-dimensional unitary matrices, for example, U_2 (Section 3), or (ii) the optimized U_N matrices (Section 4). Pros and cons of each approach will be discussed in terms of practical realizations, deterministic designs, programmability, and universality.

3 U_N operations by assembling lower-dimensional units

Given the relation $U_N^\dagger U_N = U_N U_N^\dagger = I$, a U_N matrix has N^2 degrees of freedom considering its symmetry and complex-valued components. To handle this large number of variables, a conventional approach has employed the systematic assembly of lower-dimensional unitary units, achieving deterministic design of an arbitrary U_N matrix [61]. The most widely used building block is a U_2 matrix in the SU(2) group, which is analogous to the evolution of a single qubit. In this section, we review the basic design strategy (Section 3.1) and its photonic implementations in the spatial (Section 3.2) and temporal (Section 3.3) domains.

3.1 Design strategy

In describing light behaviors in both isolated and open systems, a unitary matrix illustrates the evolutions of the couplings between optical elements, as shown in Eqs. (1) and (2). In this context, a major challenge in constructing higher-dimensional U_N matrices arises from their off-diagonal components, which necessitate the couplings between far-off elements. Because nearby interactions are dominant especially in the platforms for photonic integrated circuits whether exploiting the couplings through propagating [62] or evanescent [45] light, the basic strategy of realizing U_N is to develop the systematic assembly of nearby interactions to effectively achieve far-off couplings. Mathematically, this strategy is based on the conservation of the unitarity under the multiplications, as $(VUW)^\dagger(VUW) = I$, where U, V, and W are unitary matrices. Therefore, a common objective in this method is to achieve the diagonalization through the multiplications, as $VU_NW = D$, where D is the diagonal matrix that can be obtained simply with isolated optical elements, and V and W represent unitary matrices achievable with nearby couplings. While the target unitary matrix can be reconstructed with the multiplication form $U_N = V^\dagger DW^\dagger$, the resulting matrix multiplication corresponds to the cascaded operations exerted on light, which are executed with a series of varying optical systems along the spatial or temporal axis.

As an example, we introduce the method of implementing an arbitrary U_N using a set of two-dimensional (2D) unitary matrices U_2, which was firstly developed in Ref. [61]. For simplicity, we restrict our discussion to U_2 that reflects only the nearest-neighbor (NN) couplings in one-dimensional (1D) systems, which cover conventional programmable photonic integrated circuits using multiple waveguides [25]. To apply the unitary multiplication, we develop the N-dimensional unitary matrix T_m that includes a nontrivial 2D unitary operation U_2 at the components (m, m), $(m, m + 1)$, $(m + 1, m)$, and $(m + 1, m + 1)$, while the rest components of T_m follow the N-dimensional identity matrix I_N. The role of T_m is to cancel out an off-diagonal component through the multiplications of T_mU and UT_m, which allow for nulling one of the mth or $(m + 1)$th row and the mth or $(m + 1)$th column components, respectively (Figure 2a).

To achieve the diagonalization with a set of T_m, $N(N - 1)/2$ nulling processes applied to either the upper or lower triangular off-diagonal components are necessary (Figure 2b and c), because a triangular unitary matrix is a diagonal matrix. Therefore, in the unitary matrix reconstruction $U_N = V^\dagger DW^\dagger$, V and W are constructed with a series of NN-coupling unitaries T_m. We note that the sequence of the nulling processes supports design freedom
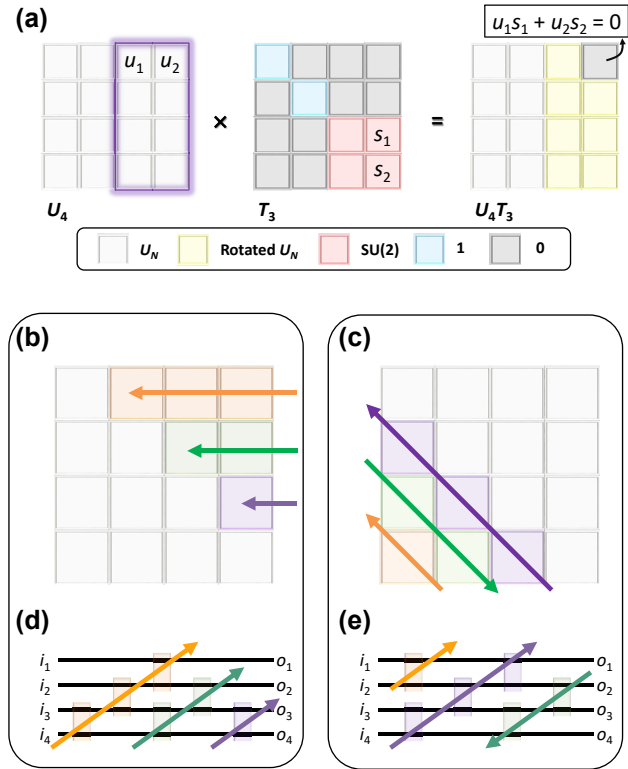

Figure 2: Universal unitaries composed of lower-dimensional units through nulling processes. (a) Example of nulling processes in the case of U_4 (components with white squares). By multiplying T_3 (red squares with SU(2) operations, blue squares with 1, and black squares with 0) on the right side of U_4, one of the U_4T_3 components becomes zero (black square) by designing the SU(2) operation to satisfy $u_1s_1 + u_2s_2 = 0$. While some of the components in U_4T_3 are identical to those in U_4, the other components are the SU(2)-transformed U_4 components. The purple box in U_4 denotes the SU(2)-transformed part. (b, c) The nulling processes of the (b) Reck [61] and (c) Clement [29] designs, and (d, e) their hardware implementations, respectively. The color of each arrow in (b, c) corresponds to the optical element of the same color in the circuits of (d, e). In (b–e), the nulling process is achieved sequentially, following the order of the orange, green, and purple arrows. The colored boxes in (d, e) represent the SU(2) building block described in Sections 3.2 and 3.3. In (d, e), i_n and o_n are the nth input and output signals, respectively $(1 \leq n \leq 4)$.

as long as a series of the cascaded nulling processes operate independently, that is, the protection of the nulled components during the subsequent processes. Representative examples include the Reck ([61], Figure 2b) and Clements ([29], Figure 2c) designs, which result in the optical hardware with different feature sizes and symmetry conditions (Figure 2d and e). Notably, owing to its structural symmetry, the Clements design achieves almost half the circuit depth and higher fidelity with error-tolerant interferences, compared to the Reck design.

The range of the unitary group accessible through nulling processes is determined by the universality of the unit unitary matrix T_m and the diagonal matrix D. Particularly, with the universal form of T_m and D, a universal set of U_N that covers random Haar matrices [63] can be achieved deterministically. Because the diagonal components of D have the unit modulus, the tailored phase evolutions in individual optical elements, such as optical waveguides or resonators with phase shifters, enables the universal form of D. Therefore, a major challenge in achieving programmable and universal U_N construction is the realization of the reconfigurable building block for T_m, which has to satisfy the complete coverage of the SU(2) group, at least, up to the global phase for nulling an arbitrary off-diagonal element during the diagonalization. In the following Sections 3.2 and 3.3, we explore the spatial- and temporal-domain realizations of T_m, which possess distinct characteristics in their design procedures and the performance figures of the resulting U_N.

3.2 Spatial domain implementation

Because T_m describes the evolution of photonic states in a two-level system up to the global phase, the corresponding operation is characterized by two degrees of freedom: the relative differences in the amplitudes and phases of the fields inside two elements [25]. As discussed in quantum computation [3], the universality of such an operation is guaranteed by a set of two arbitrary rotation operations among R_x, R_y, and R_z, which denote the rotations about x-, y-, and z-axis, respectively. These rotation operations, generally describing the θ-angle rotation about the vector $\mathbf{n}$, can be expressed as the following propagator form:

$$R_n(\theta) = \exp\left(-i\frac{\theta}{2}\mathbf{n} \cdot \boldsymbol{\sigma}\right), \qquad (3)$$

where $\boldsymbol{\sigma}$ is the Pauli vector $\boldsymbol{\sigma} = \mathbf{x}\sigma_x + \mathbf{y}\sigma_y + \mathbf{z}\sigma_z$ for the following Pauli matrices:

$$\sigma_x = \begin{bmatrix} 0 & 1 \\ 1 & 0 \end{bmatrix}, \quad \sigma_y = \begin{bmatrix} 0 & -i \\ i & 0 \end{bmatrix}, \quad \sigma_z = \begin{bmatrix} 1 & 0 \\ 0 & -1 \end{bmatrix}. \qquad (4)$$

Regarding passive and active optical elements widely used in integrated photonics, the rotation operations that are practically more accessible are R_x and R_z. First, as shown in the form of σ_x in Eq. (4), which is the generator of R_x, the rotation R_x can be obtained with the in-phase coupling between two elements, such as two coupled waveguides composing a directional coupler. The amount of the R_x rotation is then determined by the magnitude of the coupling coefficient and the length of the coupler. Second, the rotation R_z is achieved with σ_z in Eq. (4), which is achieved

with the decoupled optical elements with different on-site energies such as the propagation constants in waveguides and the resonance frequencies in resonators. To achieve arbitrary rotations of R_x and R_z, the listed optical parameters – coupling coefficient, coupler length, propagation constants, and resonance frequencies – need to be reconfigurable. It is worth mentioning that the realization of R_y, which requires the gauge field in the coupling due to the imaginary off-diagonal terms in σ_y, is not straightforward in the spatial-domain integrated photonic platforms. Instead, R_y can be obtained with a series of R_x and R_z, as $R_y(\theta) = R_x(3\pi/2)R_z(\theta)R_x(\pi/2)$.

The SU(2) gate, which conducts an arbitrary $U_2 \in$ SU(2) matrix operation for the nulling processes in Figure 2, can be realized by cascading the constituent operations R_x and R_z, as $U_2 = \Pi_k R_{n(k)}(\theta_k)$, where $n(k)$ denotes the rotation axis x or z, and k is the order index of the SU(2) operation. It is noted that the configuration of U_2, which is determined by the number and order of the rotations, is not unique. Although the simplest form of U_2 would be the straightforward multiplication of two orthogonal rotations, such as $U_2 = R_z(\theta_2)R_x(\theta_1)$ or $R_z(\theta_2)R_y(\theta_1)$, one needs to consider the practical implementation of each configuration in terms of the operation fidelity, the method for reconfigurability, and the compatibility with fabrication techniques.

Regarding the difficulty in directly implementing R_y, the most straightforward architecture employs tunable directional coupling [64]–[66] (Figure 3a and b). The tunable directional coupler corresponds to a reconfigurable R_x rotation, which enables the following relation:

$$U_2 \equiv R_z(\eta)R_x(\gamma) = \begin{bmatrix} e^{-i\frac{\eta}{2}}\cos\left(\frac{\gamma}{2}\right) & -ie^{-i\frac{\eta}{2}}\sin\left(\frac{\gamma}{2}\right) \\ -ie^{i\frac{\eta}{2}}\sin\left(\frac{\gamma}{2}\right) & e^{i\frac{\eta}{2}}\cos\left(\frac{\gamma}{2}\right) \end{bmatrix}, \quad (5)$$

where γ is the rotation angle of $0 \leq \gamma \leq \pi$ about the x-axis. Although stable manipulation of the coupling is a critical engineering issue, as discussed in below, the mathematically straightforward structure of the unit and the resulting geometrical simplicity are clear advantages of this approach.

On the other hand, the most widely used configuration involves a fixed R_x (Figure 3c and d), highlighting the technical challenges in achieving reconfigurability of coupling coefficients. To adjust the coupling for controlling $R_x(\theta)$ without affecting R_z rotations, the optical modes within the elements must be perturbed symmetrically. Furthermore, the nonlinear relationships between material perturbations and modal profiles [70]–[72], as well as between the perturbed modal profiles and coupling coefficient [73], need to
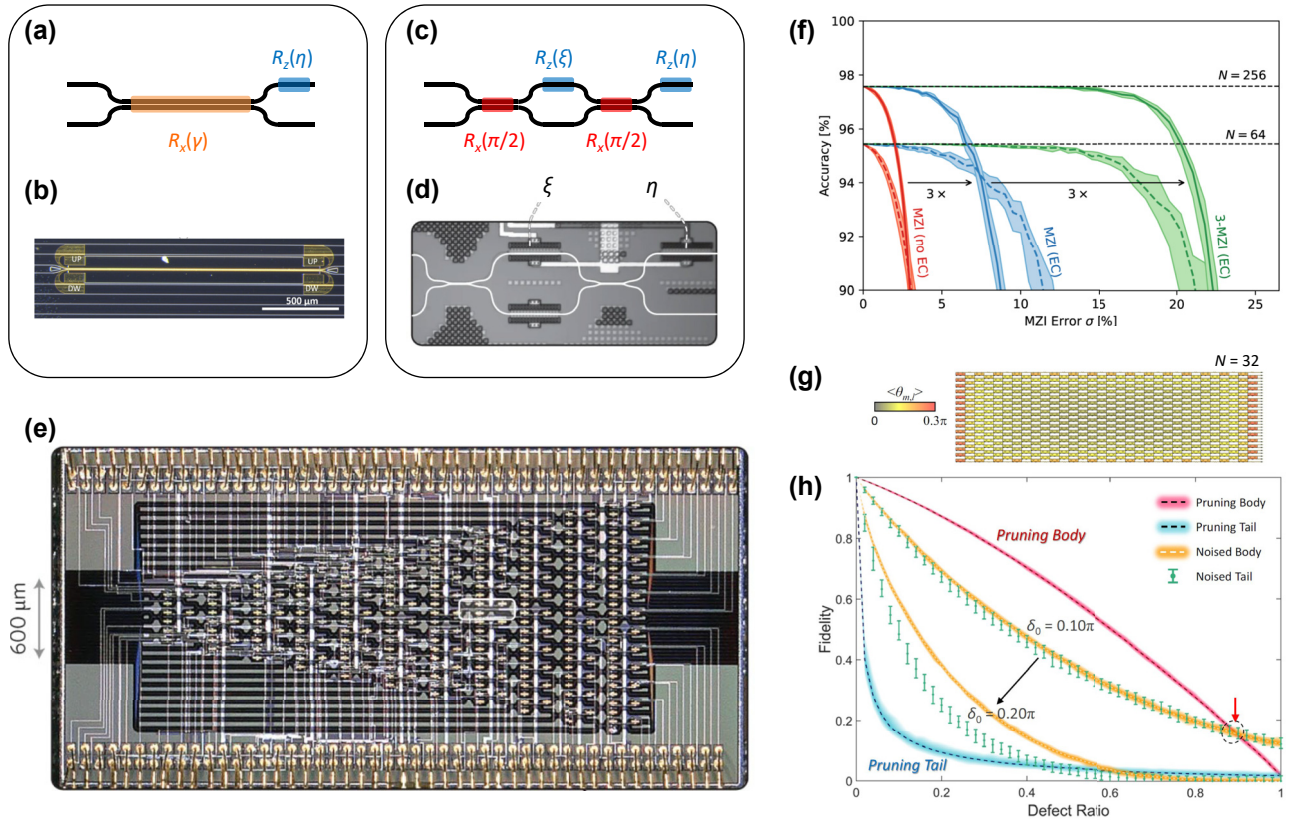
Figure 3: Spatial implementation of universal unitary circuits. (a, b) SU(2) gate with the reconfigurable R_x rotation: (a) schematic of the gate, and (b) its real implementation [64]. (c, d) SU(2) gate with the fixed R_x rotations: (c) schematic of the gate, and (d) its real implementation [10]. (e) The PPC implementation using a set of SU(2) gates in (d). (f) Effect of hardware errors on pattern recognition [67] for 28 × 28 images from the MNIST dataset [68]. 'EC' denotes the error correction achieved by the self-configuration of Mach-Zehnder interferometers (MZIs) and MZI with an additional beam splitter (3-MZI). (g, h) The pruning of PPCs for noise-resilient unitary operations [69]. (g) The averages of the phase shift $\xi = <\theta_{m,l}>$ for the PPCs of 100 U_{32} realizations. (h) Comparison of the fidelities of the U_{128} PPCs in different groups: pruning body (red line), pruning tail (blue line), noisy body (orange line), and noisy tail (green error bars). The thicknesses of the colored lines and the error bars present the range of the fidelities between their maxima and minima. Panel (b) reprinted with permission from Ref. [64], Optica. Panels (d, e) reprinted with permission from Ref. [10], Springer Nature Limited. Panels (f) and (g, h) are adapted with permission from Refs. [67], [69], respectively, Springer Nature Limited.

be mitigated. Therefore, to avoid the sensitivity and non-linearity in performing reconfigurable $R_x(\theta)$, most conventional programmable photonic circuits (PPCs) have leveraged the relationship of $R_x(\pi)R_y(\xi) = R_x(\pi/2)R_z(\xi)R_x(\pi/2)$, which leads to

$$U_2 \equiv R_z(\eta)R_x(\pi/2)R_z(\xi)R_x(\pi/2)$$

$$= \begin{bmatrix} e^{-i\frac{\eta}{2}} \sin\left(\frac{\xi}{2}\right) & e^{-i\frac{\eta}{2}} \cos\left(\frac{\xi}{2}\right) \\ e^{i\frac{\eta}{2}} \cos\left(\frac{\xi}{2}\right) & -e^{i\frac{\eta}{2}} \sin\left(\frac{\xi}{2}\right) \end{bmatrix}$$

$$= R_z(\eta)R_x(\pi)R_y(\xi). \tag{6}$$

As shown in Figure 3a and b, the corresponding SU(2) gate is composed of two identical passive Mach-Zehnder interferometers both for $R_x(\pi/2)$, and two phase shifters of

ξ and η for $R_z(\xi)$ and $R_z(\eta)$, respectively. When $0 \leq \xi \leq \pi$ and $0 \leq \eta < 2\pi$, the degrees of freedom provided by two rotations $R_z(\eta)$ and the effective $R_y(\xi)$ allow for the realization of universal SU(2) operations, completely covering the entire evolutions on the Bloch sphere. It is worth mentioning that although other configurations, such as $U_2 = R_z(\eta)R_x(3\pi/2)R_z(\xi)R_x(\pi/2) = R_z(\eta)R_y(\xi)$ that is a mathematically more concise form, are also allowed, the critical advantage of the configuration in Eq. (5) lies in the identical form of $R_x(\pi/2)$, which results in the same fabrication conditions for the Mach–Zehnder interferometers.

To achieve the necessary modulation for the reconfigurable operations of the SU(2) gate, various modulation schemes have been examined. A conventional approach involves using thermo-optic modulation [10], [65], [74]–[77], which possesses advantages of compact gate design due to substantial changes in the refractive index, and low

insertion loss. However, this approach presents several challenges, such as limited operation bandwidth of a few MHz and high-power consumption. To address each issue, various alternative solutions have been successfully demonstrated. For example, electro-optical modulation using lithium niobite films offers from 1 to 100 GHz modulation for phase shifts [78], [79]. In terms of power consumption, piezo-optomechanical techniques enable μW-scale operations per modulator with operation speeds about 100 MHz [80], [81]. Owing to the sharply different features of each modulation technique, the method of modulation is a core factor in determining the performance and application target of the entire PPC (Figure 3e).

All modulation techniques and the passive elements used in the SU(2) gate inevitably involve noise and defects. Furthermore, such random errors scale with $O(N^{1/2})$ due to the $O(N)$ circuit depth. Therefore, addressing fidelity issues through error correction is critical, especially when conducting computing functionalities in larger N, even for stochastic operation such as deep learning. Furthermore, devising hardware error correction can also be employed in the *in situ* training of deep learning in terms of the suppression of cost functions [82], [83].

To address imperfections, for example in linear-optic elements such as beam splitters, various systematic calibration procedures have been developed. In these procedures, the underlying mechanisms are developed upon two notions: measurement-based reconfigurability and the utilization of auxiliary dimensions within system parameter spaces. First, error correction necessitates both signal detection and the consequent reconfiguration of systems. Although an individual correction of each element is expected to be ideal for high fidelity [28], [84]–[87], such an ideal condition not only burdens the fabrication difficulty but also raises additional noises due to the necessity of local signal monitoring. Therefore, there have been substantial efforts on reducing the required number of internal detectors and tunable elements. The approach at the extreme is global optimization, for example, using gradient descent [88] or the *in situ* training with adjoint optimization, which requires only detecting signals at the system boundaries [82], [83]. The challenge of employing these techniques to error correction would be the difficulty in properly setting initial conditions to explore global optimum and the necessity of problem-specific training. Recently, error correction without internal detectors for sufficiently low local errors has been demonstrated using self-configuration method, which corrects the splitting error in each beam splitter [89]–[91].

Another approach – auxiliary dimensions in system parameter spaces – increases the upper bound of accuracy at a given level of device defects. At an elemental level, it was demonstrated that a beam splitter targeting 50:50 power division but with errors up to 85:15 can be adjusted by doubling the system dimension through additional phase shifters and beam splitters [28]. In a similar context, employing additional passive elements to each gate, such as a beam splitter and waveguide crossing, allows for avoiding forbidden regions in the Hilbert space of optical states [67]. This improved coverage enhances the accuracy of the circuit operations (Figure 3f) beyond previous works [89]–[91], achieving fault tolerant pattern recognition. The use of auxiliary dimension has also been employed in system levels, such as the realization of random Haar matrices using an additional beam splitter layer at the terminal port of the photonic circuit [92].

In a similar context, a method inspired by network science has recently been proposed, focusing on categorizing active optical elements based on their impacts on achieving reconfigurable universal unitary operations [69]. The work demonstrated that the building blocks of PPCs designed under the Clements approach [29] for achieving random Haar matrices follow the power law and the Pareto principle, stating that most of the significant rotation operations come from about 20 % of the building blocks – the 'tail' elements of the circuit. This analysis inspires the pruning of less important phase shifters in the overall circuit (Figure 3g), which enables the removal of tunable phase shifters that are usually the most expensive elements in PPCs in terms of noise and footprint engineering. As shown in Figure 3h, pruning the 'body' of the phase shifters – less important ones, constituting about 80 % of the circuit – can yield even better performance at a specific level of noise, aligning with the underlying mechanisms of hub nodes in network science [93]. Recently, the concept of pruning for photonic circuits has also been employed in relation to the training process [94], [95], achieving reduced power consumption and noise resilience.

3.3 Temporal domain implementation

Despite the great success of spatial-domain PPCs especially in terms of fidelity [28], [31], [67], [69], [82], [86]–[92], [96], [97], scalability remains another critical challenge. To diagonalize a U_N matrix using SU(2) operations, $N(N-1)/2$ nulling processes are necessary as described in Figure 2. Even when approximately $N/2$ operations are achieved in parallel, as is available in the Clements design [29], the circuit depth is proportional to N, which results in $O(N^2)$ scalability in both device footprint and gate number regarding the channel number N. This poor scalability, for example, requiring over 10^6 elements with footprints exceeding a few cm^2 for a deep

learning model with only 1,000 neurons, also raises substantial fidelity issue due to imperfections in device fabrication and light sources.

One possible approach to overcoming this limitation is to exploit the mathematical similarity between the governing equations in different physical axes. For example, the spatial propagation of light along a waveguide and the temporal evolution inside a resonator can be described by the almost same equations of $da/dx = -i\beta a$ and $da/dt = +i\omega a$ [73], respectively, where a is a field amplitude, β is the wavenumber along the waveguide, and ω is the resonance frequency of the resonator. Therefore, one can replace the field evolution of light along the spatial domain with the evolution along an alternative physical axis – time or frequency – which allows for the substitution of the device footprint with the operation time or mode number. Similar approaches have been employed in examining synthetic-dimensional phenomena [13], [98]–[103], supersymmetric transformation [104], crystal optics [39], [105], and disordered photonics [41], [43].

The proposal of programmable unitary circuits using temporal-axis computation, referred to as programmable photonic time circuits (PPTCs) [106], corresponds to the space-to-time replacement of wave evolutions to address the poor footprint scalability of PPCs. The underlying mechanism of PPTCs relies on tailoring optical spatial modes using time-domain modulation, which has been intensively studied in various platforms. For example, recent studies on photonic time crystals [39], [105] and time disorder [40], [41], [43] have focused on controlling directivity of light with broken continuous time translational symmetry while preserving spatial translational symmetry. The simultaneous breaking of spatial and time translational symmetry allows for advanced manipulation of optical modes, such as wavelength conversion [107], complete optical isolation [108], effective magnetic fields [109], and non-Hermitian band manipulation [110]. In line with these historical cornerstones, the goal of PPTCs is to achieve reconfigurable and universal unitary operations of optical spatial modes using broken spatial and time translational symmetries in integrated photonic platforms, by adjusting the design strategy of PPCs.

In PPTCs, the nulling process for diagonalization is identical to the spatial counterpart, while the spatial SU(2) gate is replaced with the temporal one. This SU(2) 'time gate' consists of two identical travelling-wave resonators with resonance frequency ω_0 (Figure 4a) to describe two-level systems with the spinor state $\Psi = [\psi_m, \psi_n]^T$, where ψ_m and
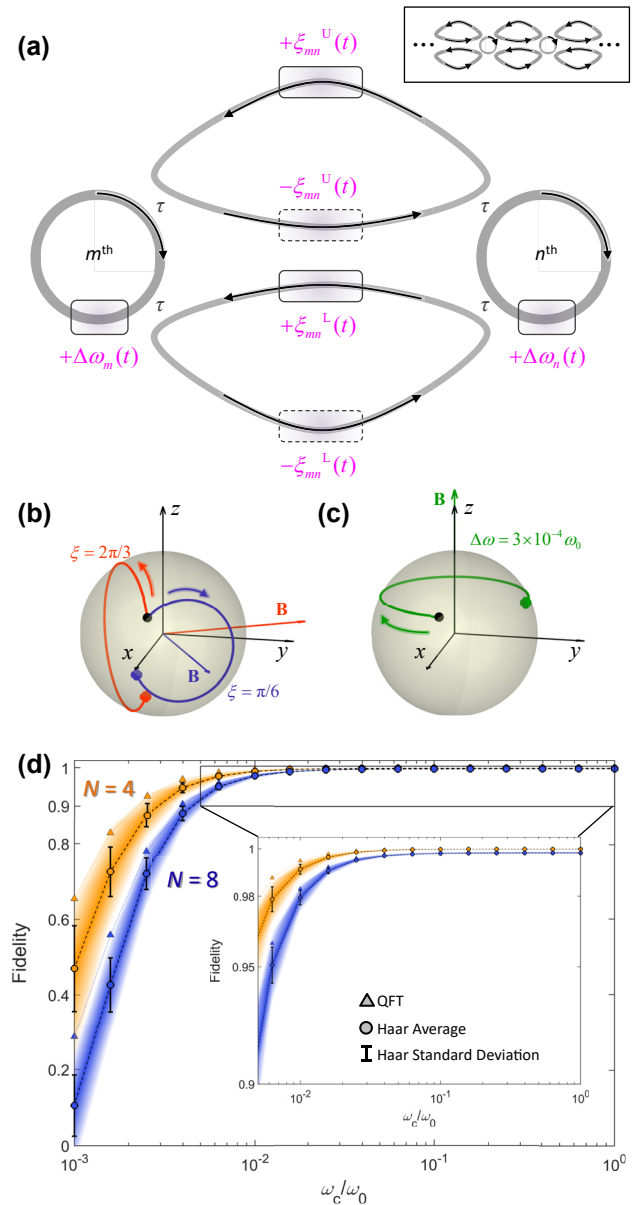

Figure 4: Temporal implementation of universal unitary circuits.
(a) The SU(2) time gate between the mth and nth channels. Gray circles and curved triangles represent resonators and waveguide loops, respectively. Purple boxes are phase shifters. The upper right inset illustrates a PPTC comprised of multiple SU(2) time gates. (b, c) Temporal evolution of pseudospinor modes on the Bloch sphere for two operation modes: (b) even-parity mode for $\xi_{mn}^U(t) = \xi_{mn}^L(t) = \xi$ and $\Delta\omega(t) = 0$ in (a), and (c) odd-parity mode for $\xi_{mn}^U(t) = -\xi_{mn}^L(t) = \pi/2$ and $\Delta\omega(t) \neq 0$ in (a). **B** denotes the pseudospinor rotation axis. (d) PPTC fidelities with respect to the cutoff frequency ω_c of low-pass filtering. Circles and error bars represent the average and standard deviation of 20 realizations of random Haar matrices at each ω_c and triangles represent quantum Fourier transforms for $N = 4$ (two qubits; orange) and $N = 8$ (three qubits; blue). Panels (a–d) reprinted with permission from Ref. [106], APS.

ψ_n are the field amplitudes of the specific pseudospin modes in the neighboring mth and nth resonators, respectively. The resonators are coupled via a pair of single-mode waveguide loops with a decay rate $1/\tau$, which have been widely employed in topological photonics to achieve pseudogauge fields in coupling [34], [111], [112]. When preparing tunable phase shifters in the resonators and waveguide loops, the spinor state is governed by the following spinor Hamiltonian [106]:

$$H_S = -\omega_0\sigma_0 - \frac{1}{2\tau}\left[\cos\,\xi_{mn}^U(t) + \cos\,\xi_{mn}^L(t)\right]\sigma_x$$
$$- \frac{1}{2\tau}\left[\sin\,\xi_{mn}^U(t) + \sin\,\xi_{mn}^L(t)\right]\sigma_y - \Delta\omega(t)\sigma_z, \quad (7)$$

where $\xi_{mn}^U(t)$ and $\xi_{mn}^L(t)$ are the time-varying phase shifts in the upper and lower loops, and $\Delta\omega$ is the time-varying averaged resonance perturbation due to the tunable phase shifters in each resonator. Equation (7) shows that the full degrees of freedom for the rotation operations, $R_{x,y,z}$, are accessible with the SU(2) time gate. By imposing the digital modulation on tunable phase shifters, the rotation operations about an arbitrary axis on the xy-plane (Figure 4b) and about the z-axis (Figure 4c) can be realized, comprising a universal set for the unitary operation of a spinor state. Such a universal SU(2) operation facilitates the extension to universal and reconfigurable U_N operations following the method described in Section 3.1, as demonstrated in the realization of the quantum Fourier transform and random Haar matrices [106], and the emulation of light behaviors inside hyperbolic lattices [113]. Because the computation is achieved with light stored inside coupled resonators, the PPTC can be understood as compressing the spatial circuit depth from N to 1, by transferring the domain for necessary computations to the temporal axis. When considering the conventional integration level of cutting-edge photonic circuits – about 10^4 gates within a cm²-scale chip [45], [111] – the potential to reduce spatial footprint using PPTCs sheds light on realizing very-large-scale integration for light-based matrix computations. The design strategy with tunable gauge fields in PPTCs has recently been extended to the implementation of integrated photonic platforms for reconfigurable matrix-valued gauge fields and the following programmable non-Abelian physics and braiding [114], which revealed novel topological phases in photonic lattices.

Remaining issues in the practical implementation of PPTCs lie in the design of modulation signals and the limitations in modulation speed. Because Eq. (7) is nonlinear, the calculation of the required phase shifts generally does not yield an analytical solution. In Ref. [106], digital modulation is applied as an analogy of the discretized building blocks in spatial-domain PPCs. However, because the speed of temporal modulation is limited by the response time of materials, ideal discretization in the PPTC is actually unattainable, and therefore, the fidelity significantly degrades with slower modulation of phase shifts (Figure 4d). The solution to this issue can be found in digital signal processing techniques [106], such as predistortion [115], and analog computation [116]–[120].

A more critical issue would be the necessity of ultrahigh quality (Q-) factors that should guarantee the storage of light during modulation. Notably, because the SU(2) gate is executed sequentially in previous works [106], [113] due to the lack of synchronization between SU(2) time gates, the resulting scalability of the necessary time period scales as $O(N^2)$. Therefore, given ultra-high quality factor of $Q > 10^8$ achieved in all-waveguide resonators [121], which enforces the termination of the entire operations inside the PPTC within about 10 ns, the lower bound of the modulation speed becomes about $(N^2/10)$ GHz for $U(N)$ operations. The realization of parallel SU(2) operations, analogous to the spatial implementation [29], [61], can substantially mitigate this problem, facilitating $O(N)$ scalability. Dynamical control of coupling quality factors [122] can also provide an optimum solution by restricting unwanted dissipation to the intrinsic loss of resonators.

4 U_N operations by cascading higher-dimensional cells

Although the assembly of lower-dimensional unitary units allows for the deterministic implementation of a higher-dimensional U_N matrix in photonic systems, the resulting architecture of the circuit is nonunique, even when we employ an identical form of unitary gates, as demonstrated in various previous works [29], [30], [61]. Therefore, the assembly introduced in Section 3 does not guarantee the optimal design for practical implementation in terms of the device footprint, gate number, signal fidelity, and the geometrical complexity of the design. This limitation inspires the necessity of developing optimization techniques to explore a global optimum by simultaneously accessing the full N^2 degrees of freedom of U_N. In this section, we review a representative example in this field – the realization of high-dimensional universal unitary operations through the cascaded unit cells of the same dimension – focusing on the basic design strategy (Section 4.1), and the implementations in the spatial (Section 4.2) and frequency (Section 4.3) domains.

4.1 Design strategy

Although the detailed design process described in this section is distinct from that in Section 3, the underlying philosophy is identical: constructing the entire $U(N)$ group with N^2 degrees of freedom from the layers of $U(N)$ subsets that are physically allowed in terms of nearby interactions. The difference lies in the dimensionality of the nontrivial parts of $U(N)$ layers. In Section 3, we introduced the use of two-dimensional SU(2) operations while the other channels experience $U(1)$ evolution. In this section, we focused on the use of N-dimensional operations, which can be implemented through nearby interactions. Consider the realization of N-dimensional universal unitary operations U using the N-dimensional cascaded unitary unit cells V_m ($m = 1$, 2, …, M; Figure 5a), as $U = V_M V_{M-1}, …, V_2 V_1$, while V_m does not need to be universal. The first step in covering N^2 degrees of freedom of U is to devise a photonic unit cell that provides V_m through nearby interactions, because achieving long-range interactions is challenging on conventional integrated platforms. By performing cascaded multiplications of V_m, we can then obtain the corresponding photonic hardware that approximates U through the substantially enhanced degrees of freedom.

In this approach toward universal unitaries, the first example of V_m is the unit cell that conducts Fourier-transform operations in the spatial domain. Various photonic systems can operate as gates for the Fourier transform of optical information, which is a subclass of N-dimensional unitary operations deterministically accessible with nearby interactions between optical elements. A representative example is a diffractive optical system, where light propagation in the Fraunhofer regime leads to the Fourier transform of the transverse profile of an optical field [38]. As a theoretical background, it was demonstrated that a reconfigurable y-axis rotation operation on the Bloch sphere of an arbitrary pair of channels can be achieved by using an N-channel discrete Fourier transform in conjunction with an N-channel diagonal unitary operation [57]. Because the diagonal unitary operation permits tunable z-axis rotations for any pair of channels, the combination of a set of Fourier-transforming (U_{FT}) and diagonal (D) unitary operations enables the configuration of the universal SU(2) operation for each pair of channels, as well as the subsequent N-dimensional unitary operations as demonstrated in Section 3 (Figure 5b).

It is important to note that the Fourier transform is not the only high-dimensional configuration suitable for constructing universal unitaries. Any form of reflectionless transfer matrix can serve as the unit cell for composing universal U_N (Figure 5c). Although such transfer matrices in
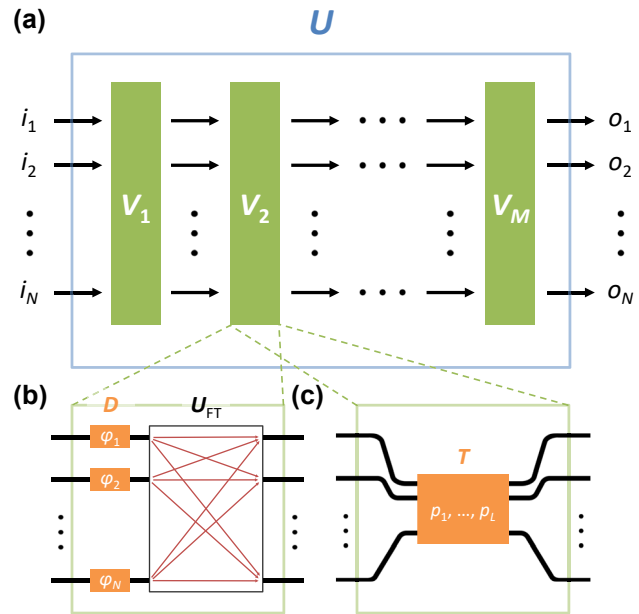
Figure 5: Universal unitaries composed of higher-dimensional cells through numerical optimization. (a) The circuit realizing universal unitary operations U. i_n and o_n are the nth input and output signals, respectively ($1 \leq n \leq N$). V_m is the reconfigurable N-dimensional unitary unit cell ($1 \leq m \leq M$) of which the operation is determined by nearby interactions accessible with integrated photonic platforms. (b, c) Detailed implementation of V_m cell. (b) V_m composed of the diagonal unitary operation D and the Fourier transform U_{FT}. The diagonal unitary matrix is realized with an array of phase shifters: φ_n for the phase shift applied to the nth channel. (c) V_m realized through the transfer matrix T, which depends on L real-valued parameters p_l ($1 \leq l \leq L$).

integrated platforms are typically characterized by nearby interactions, long-range interactions can also be achievable using specific platforms. A particularly interesting example involves employing the concept of synthetic dimensions [13], [98]–[103] to construct the unit transfer matrix using higher-order couplings. This approach also replaces spatial degrees of freedom with the frequency axis for enhanced scalability in footprint and element number, as similar to the approach in Section 3.3.

In the following Sections 4.2 and 4.3, we explore the realizations of V_m using the Fourier transform in the spatial domain and the transfer matrix in the frequency synthetic-dimensional domain, discussing their theoretical background, numerical assessment, and practical implementation.

4.2 Spatial Fourier implementation

In integrated photonics, which leverages nearby interactions between guided lights in 2D platforms, the Fourier

transform is implemented upon the concept of the fractional Fourier transform (FrFT) [123], a generalization of the standard Fourier transform. Because the Fourier transform operator and its generalization, the FrFT operator, are both unitary, their physical implementations rely on exploring Hermitian Hamiltonians of which the propagators correspond to these operators. Consider the following operator representation of the 1D Fourier transform:

$$F[f(x)] = \frac{1}{\sqrt{2\pi}} \int_{-\infty}^{\infty} f(x') \, e^{-ixx'} \, dx', \qquad (8)$$

where the conventional expression of the Fourier transform of $f(x)$ is obtained by applying F to $f(x)$, and then, replacing x at the right side of the equation with the wavenumber k. The underlying concept of the FrFT involves interpreting the Fourier transform operator F as $F = F(\pi/4)$, as described in below. As shown in Ref. [123], the operator F satisfies the following eigenvalue equation:

$$Fe^{-x^2/2}H_n(x) = e^{-in(\pi/2)}e^{-x^2/2}H_n(x), \qquad (9)$$

where $H_n(x)$ is the Hermite polynomial of order n. Notably, the eigenmodes in Eq. (9) are familiar in quantum mechanics, because they are the eigenmodes of the harmonic oscillator Hamiltonian:

$$H = -\frac{d^2}{dx^2} + x^2 - 1, \qquad (10)$$

while the eigenvalue of the Hamiltonian is $2n$. Regarding that F is a unitary operator, the Fourier transform can be considered the unitary propagator of the harmonic oscillator Hamiltonian according to the Stone's theorem [2]. From Eq. (1), the propagator applied to the nth eigenmode is $\exp(-iH\xi) = \exp(-2in\xi)$, which leads to $\exp(-in\pi/2)$ at $\xi = \pi/4$. Because this relationship is established for all the eigenmodes independent of n, the Hamiltonian of Eq. (10) provides the Fourier transform of an arbitrary state $\psi(\xi_0)$ exactly at $\psi(\xi_0 + \pi/4)$ from Eq. (9), allowing for introducing the relation $F = F(\pi/4)$ (Figure 6a). A generalized propagator $F(\xi)$, which leads to $\exp(-iH\xi)$ for the Hamiltonian H in Eq. (10), then satisfies:

$$F(\xi)e^{-x^2/2}H_n(x) = e^{-i2n\xi}e^{-x^2/2}H_n(x). \qquad (11)$$

This unitary propagator $F(\xi)$ corresponds to the FrFT operator, which includes the Fourier transform as the special case when $F(\xi = \pi/4)$. The graphical illustration of Eq. (11) in phase space is shown in Figure 6b.

Equations (10) and (11) demonstrate that the optical implementation of a harmonic oscillator potential enables light-based computing of both the Fourier transform and FrFT. According to the mathematical similarity between the Schrödinger equation and the optical paraxial wave equation [6], [7], the harmonic oscillator potential can be readily obtained by engineering an effective refractive index profile [126]–[128]. Because a higher refractive index corresponds to a lower quantum potential, the index profile of optical harmonic oscillators is shaped like a convex lens, with a higher index around the center.

In integrated photonics, achieving a continuous variation of the refractive index could be challenging because the unit elements, such as optical waveguides or resonators, are usually discretized with fixed geometrical and material specifications. Therefore, a common approach lies in realizing the discrete fractional Fourier transform (DFrFT) [129], which corresponds to the generalization of a discrete Fourier transform. Because harmonic oscillators can also be effectively reproduced in discretized systems, such as waveguide arrays with detuned coupling or propagation vectors [130]–[132], the DFrFT and its special case of the discrete Fourier transform can be implemented by tailoring the evolution parameter ξ within optical harmonic oscillators (Figure 6c) [124].

The DFrFT on integrated photonic platforms has been intensively studied to realize light-based computing by performing universal unitary operations [133], [134], convolution operations [135], and arbitrary linear operations [125] (Figure 6d–f). Although it has been demonstrated that universal unitary operations can be obtained through alternating multiplications of diagonal unitary matrices and Fourier-transforming (U_{FT}) matrices [57], designing the diagonal matrices and determining the number of unit cells (M in Figures 5a and 6e and f) still requires numerical assessments. Recently, a more general form, involving the DFrFT instead of the discrete Fourier transform, was used to obtain universal unitary operations [133]. In this approach, numerical optimization with the Levenberg-Marquardt algorithm [136], [137] was employed to inversely design diagonal unitary matrices, which correspond to the phase-shifting layers (D in Figure 5b). The result demonstrates that ($N + 1$) phase-shifting layers are sufficient to reproduce universal unitary operations approximately, resulting in $O(N^2)$ scalability both for the footprint and element number, similar to the SU(2)-based design in Section 3.2. Although the design has yet to demonstrate superior scalability, its more simplified geometry without Mach–Zehnder interferometers could be advantageous especially in large-scale realizations. Furthermore, because the design is defect-resilient, maintaining the universality with one faulted phase shifter at each layer, an extended comparison with the SU(2)-based design will be necessary in future studies. It is worth
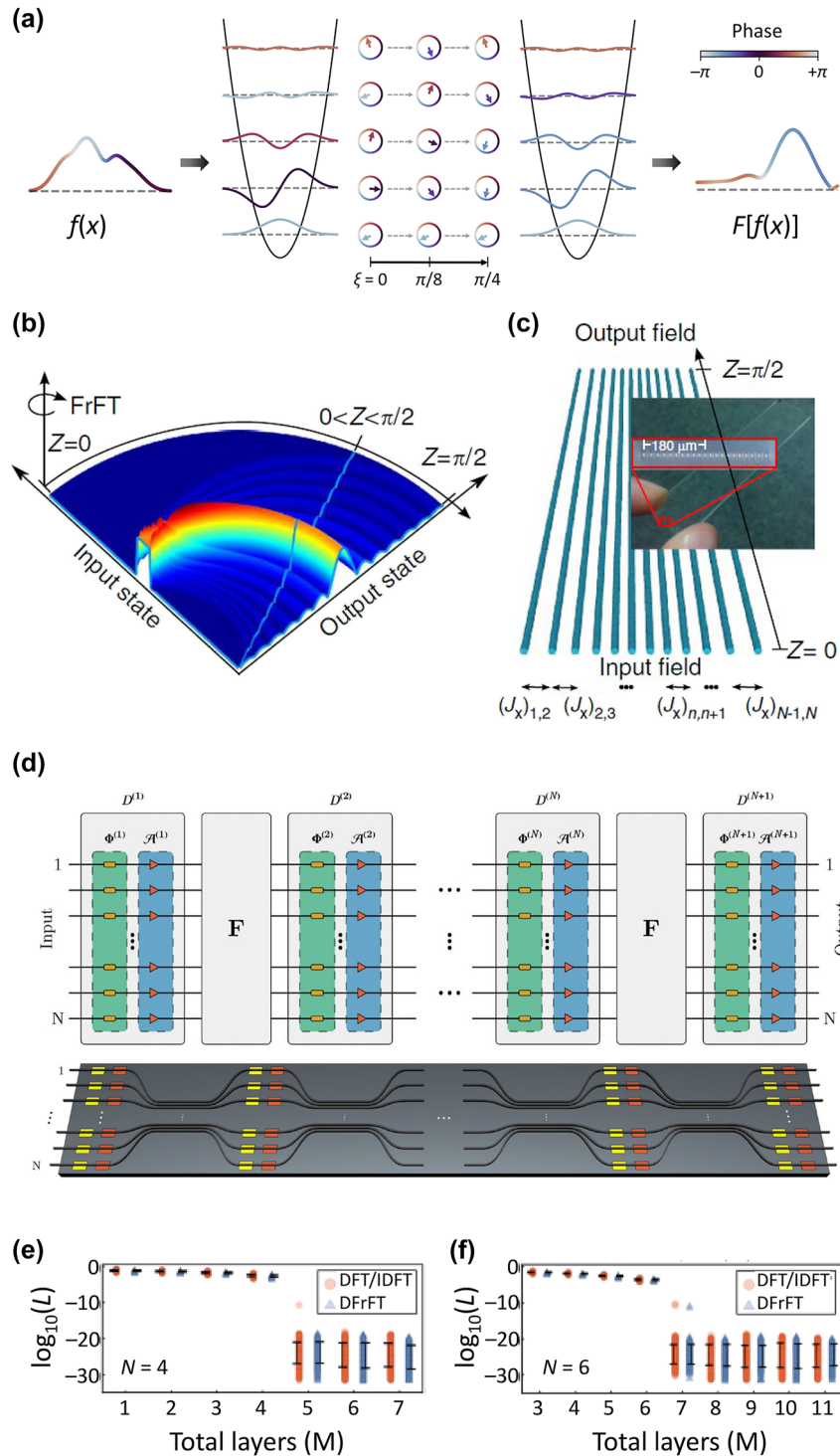
Figure 6: Spatial Fourier implementation of universal unitary circuits. (a) Schematic for illustrating the Fourier transform achieved through wave evolution in a harmonic oscillator potential. The arrows connecting colored circles represent the phase evolution of each eigenmode through the propagator $\exp(-2in\xi)$. (b) Pictorial view of FrFT in phase space, where $Z = 2\xi$ in Eq. (11). (c) A schematic of an engineered waveguide array for an optical harmonic oscillator potential. (d) Schematic for the proposed decomposition of universal linear $N \times N$ matrices with the complex diagonal matrices $D^{(m)}$ and the DFrFT matrix F. The diagonal matrices are further decomposed into a layer of phase shifters $\Phi^{(m)}$ and a layer of amplitude modulators $A^{(m)}$. Schematic of a photonic-device architecture is shown in the bottom figure. (e, f) Errors L in reproducing universal linear matrices for (e) $N = 4$ and (f) $N = 6$, while varying the total number of layers M. Panels (b, c) reprinted with permission from Ref. [124], Springer Nature Limited. Panels (d–f) reprinted with permission from Ref. [125], APS.

mentioning that alternating multiplications of the Fourier transform, a complex-valued diagonal matrix, and the inverse Fourier transform allow for the construction of circulant matrices [138], enabling the realization of an arbitrary complex matrix [139]. In this context, the approach in Ref. [133] has recently been generalized to universal linear operations using the DFrFT [125], which can be directly applied to weight matrices in photonic deep learning and application devices, such as real-time optical direction-finding sensors [140]. In terms of resolving scalability, the utilization of the FrFT in the time domain [141] for constructing unitary operations can be a topic of future studies, as the correspondence of the relationship between PPCs in Section 3.2 and PPTCs in Section 3.3.

4.3 Synthetic-dimensional implementation

Despite the simplified and defect-resilient design using the spatial-domain DFrFT, the overall scalability of the footprint and element number remains $O(N^2)$, which hinders large-scale implementations required for deep-learning applications. Similar to the utilization of the temporal axis in Ref. [106], employing computation on alternative physical axes instead of the spatial domain also became necessary in unitary operations using higher-dimensional unit cells. One approach is to utilize the synthetic frequency dimension [100], [142].

The concept of the synthetic dimension allows for exploring light behaviors in higher-dimensional spaces beyond the spatial dimension by exploiting internal degrees of freedom of photons or imposing extended system parameters on the governing Hamiltonian [100]. Figure 7a illustrates an example of the first approach: the use of multimode optical resonances within a single ring resonator, which extends a zero-dimensional (0D) photonic structure to an effective 1D or higher-dimensional system. The key mechanism relies on the analogy between signal transport along a spatial axis and coupling across multiple optical modes, enabling the frequency axis, which represents resonance modes, to be considered as a synthetic dimension. Because resonance modes are initially orthogonal to each other in both the spatial and temporal domains, such coupling can be achieved through spatio-temporal modulation to break this orthogonality, for example, by finite-space modulation for broken spatial orthogonality [107], and at the same time, by designed temporal modulation to control frequency-domain coupling distributions [98], [143]–[145]. In this field, electro-optical modulators (EOM) have been widely employed for their sufficiently large modulation speed and depth, which determine the accessible range of the free-spectral range (FSR), the accessible orders of

neighboring couplings, and the coupling strength. The synthetic dimension has been widely applied in topological photonics, permitting the observation of three- [13] or even four-dimensional [142] topological phenomena in 2D integrated photonic platforms, with the experimental verification of the concept [101], [146].

Employing the extended dimension from the concept of the frequency-synthetic dimension, $O(N)$-scalable implementation of universal unitary operations has been recently demonstrated (Figure 7b) [147], which can be generalized to arbitrary linear transformations. In the proposed system, superior scalability is achieved by compressing the spatial circuit width from N to 1, which is obtained by replacing N-channel operations with a higher-dimensional N-element lattice unit cell developed in the 0D resonator. Each basis vector for matrix operations corresponds to the resonance mode, $\omega_m = \omega_0 + m\Omega_R$, where m is an integer, ω_0 is the reference frequency, and Ω_R denotes the FSR. To configure the lattice, the EOM modulates the permittivity in the finite region of the resonator through a combination of multiple harmonics, as $\Delta\varepsilon = \Sigma_l \, \delta\varepsilon_l \cos(l\Omega_R t + \theta_l)$ $(1 \le l \le N_f)$, where $\delta\varepsilon_l$ and θ_l are the modulation depth and phase for the modulation frequency $l\Omega_R$, respectively. We note that l values greater than 1 enable long-range couplings, which are one of the critical advantages of utilizing synthetic dimensions compared to the intricate design required for spatial long-range coupling [148]. Such long-range couplings allow for the efficient access to off-diagonal elements in matrix operations, providing higher-dimensional unit cells with excellent expressivity for constructing universal unitaries. The dimensionality N of unitary operations is defined by establishing spectral boundaries that block undesired couplings into too higher- or lower-modes, which can be realized with inner auxiliary rings. The rings split the modes outside the spectral boundaries through the coupling process, which deviates eigenfrequencies, and thus, results in decoupling (Figure 7c) [101].

To fulfill the necessary degrees of freedom required for unitary operations, the entire system consists of an array of N_r unit cells, each performing an N-dimensional unitary transfer matrix T (Figures 5c and 7b). The unit cell is composed of a synthetic-dimensional ring resonator side-coupled to an external waveguide. Across each unit cell, the waveguide supports the $N \times 1$ input mode vector $s^+ = [\ldots, s_{-1}^+, s_0^+, s_1^+, \ldots]^T$ and the $N \times 1$ output mode vector $s^- = [\ldots, s_{-1}^-, s_0^-, s_1^-, \ldots]^T$, where s_m^+ and s_m^- are the input and output modes, respectively, which are coupled with the resonance mode at ω_m. The unit cell then conducts a unitary operation of $s^- = Ts^+$. Notably, the circuit depth N_r is determined by the entire degrees of freedom in
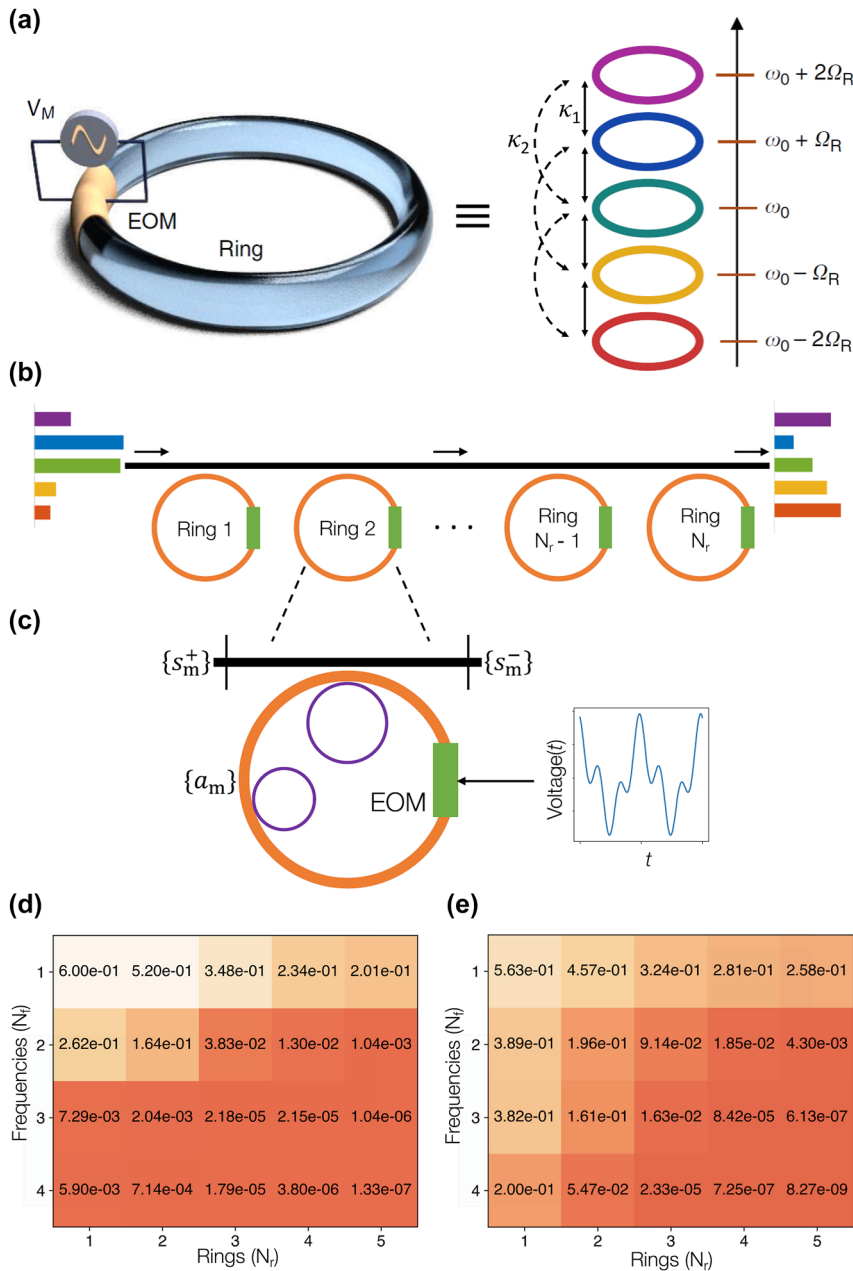
Figure 7: Synthetic-dimensional implementation of universal unitary circuits. (a) Dynamically modulated ring resonator and its band structure for comprising the synthetic frequency dimension. The resonator is modulated via the multiple harmonic signal V_M applied to a part of the ring (left), which can create nearest-neighbor (κ_1) or long-range (κ_2) coupling (right). 'EOM' denotes an electro-optic phase modulator. (b) The entire system for generating universal unitary operations and the subsequent arbitrary linear transformations. The input is encoded in five-dimensional frequency modes. (c) A unit cell design. The dielectric property of the ring resonator is controlled through the multiple harmonic EOM signal, which allows for the reconfigurable unitary transfer matrix applied to the input profile $\{s_m^+\}$. The purple rings represent the internal auxiliary rings for creating frequency boundaries. (d, e) The errors as functions of the number of the unit cells N_r and the number of modulation harmonics N_f in obtaining a five-dimensional (d) permutation matrix and (e) Vandermonde matrix. Panels (a) reprinted with permission from Ref. [146], Springer Nature Limited. Panels (b–e) reprinted with permission from Ref. [147], Springer Nature Limited.

multiple harmonic modulations $2N_f$ from $\delta\varepsilon_l$ and θ_l, and the dimensionality N, enforcing the condition of $2N_f N_r \geq N^2$ for universality. As similar to the optimization process in Section 4.2, this synthetic-dimensional resonator array

is inversely designed using a gradient-based procedure: the limited-memory Broyden–Fletcher–Goldfarb–Shanno algorithm [149]. In contrast to the spatial- or temporal-domain realizations treated in Sections 3.1, 3.2, and 4.2, the

unitary transformations in this system are non-reciprocal due to the spatio-temporal modulations [108], [150]. An arbitrary linear transformation was also examined by exploiting the sub-dimensional space of the system for unitary operations [151].

When compared with the PPTC [106], which also achieves $O(N)$ scalability through the transfer of the circuit depth into the temporal axis, the synthetic-dimensional approach that transfers the circuit width to the frequency axis allows for a more mitigated condition on computing time [147], because each resonator needs to store light during $1/N$ part of the entire computation. Nonetheless, we note that the synthetic-dimensional system requires equally-spaced multi-wavelength sources and detectors due to its operation principles, which could compose a challenge in the extension to large-scale integrated systems. For example, because the number of modulation frequencies, N_f, should be comparable to N for universal unitaries within $O(N)$ spatial footprint, the system requires both high modulation frequencies and small FSRs. Although lithium-niobate phase modulators offer modulation bandwidths of about 100 GHz [78], the realization of $N = 1,000$ synthetic-dimensional systems necessitates FSRs of the order of 100 MHz. Therefore, the recent experimental demonstration of synthetic-dimensional systems has mainly implemented in fiber optic platforms, which allow for meter-scale optical resonators [101], [144]. Recent achievement of realizing meter-scale delay lines on a mm^2-scale photonic chip can be applied to synthetic-dimensional computing in integrated photonic platforms [152].

5 Conclusions and outlook

After emphasizing the ubiquitous nature of unitary operations in photonics, we explored the design methods for photonic unitary circuits, which enable ultrafast, reconfigurable, and universal unitary operations necessary for light-based computing. We categorized these methods into two groups based on the dimensionality of the building block operations – analytical design using lower-dimensional ones, such as SU(2) operations, and numerical optimization using higher-dimensional ones, such as Fourier transforms. The methods of each group possess different pros and cons.

When lower-dimensional operations, especially SU(2) ones, are employed to compose unitaries, theoretically perfect forms of unitary operations are accomplished systematically. Therefore, this approach allows for more precise computing applications without theoretical defects in principle, enabling the selective engineering of unit cells, such as the calibration to experimental defects [96] and the design of

the fault-tolerant geometry [67], [69]. However, because the method itself does not guarantee the optimized configuration in terms of the fidelity, device footprint, and element number, employing a more superior geometry [29], [30] or utilizing other wave degrees of freedom [106] remains an ongoing research topic.

In comparison, the approaches employing higher-dimensional building blocks inevitably utilize numerical recipes due to extended parameter spaces. Therefore, the realization of the perfect fidelity becomes more challenging than the SU(2)-based approach, especially when considering the possible existence of local minima. However, as shown in the DFrFT unit cell [125], [133], [134], this approach can provide more simplified geometry that could be preferred in real implementations. Furthermore, the Fourier-based realization can offer more efficient routes to advanced functionalities, such as convolutional operations [135] and Fourier-space computation [153].

Remaining critical issues in performing unitary-based computations with integrated photonic hardware include achieving scalability below $O(N)$, ensuring high fidelity against defects, exploring global optima in the circuit design, and achieving nonlinearity for advanced functionalities. First, as demonstrated by approaches exploiting temporal [106] and frequency [147] axes, potential solutions for scalability may be found in utilizing the rich internal degrees of freedom of light, such as polarizations and orbital angular momenta. In this context, the application of metamaterials to integrated photonics, such as metatronics [117], [154], can offer a novel solution for increasing the overall information capacity within a limited footprint. Another route may involve the construction of complex network architecture for light [155], [156], which can provide more efficient access to off-diagonal elements through far-off coupling, thereby enabling a compact design. A promising solution to this issue lies in the utilization of quantum states, which allow the dimensionality of the Hilbert space to increase exponentially with the number of particles [3].

Many recent studies have focused on achieving unitary operations with partially coherent light [157]–[160], which accommodates more practical scenarios. In addition to the use of feedback-based self-configuring systems to manage partial coherence [160], researches on dynamical stable theory [161]–[164] and topological phenomena [112], [165] in view of unitary operations could be a future research topic to achieve internal fault tolerance as analogous to topological computation by anyonic operations [166].

In leveraging higher-dimensional unit cells to optimize photonic unitary circuits, the expanded system dimensionality and increased coupling complexity substantially raise

the difficulty of finding a global optimum within the parameter space. Given the recent surge of interest in using deep learning to design electronic chips [167], we can envisage the application of data-driven approaches to the design of high-dimensional photonic unitary circuits. Such an approach would enable the use of complex optical materials [156], [168] for reconfigurable and universal unitary operations, without relying on analytically solvable forms. Although gradient-based approaches, including deep learning for photonic system design [169]–[173], offer rapid convergence to local minima, designing large-scale photonic circuits may require methods better suited for finding a global optimum, such as neuroevolution [174], [175], particle swarm optimization [176], adjoint-based design [177], [178], and a global optimizer using a conditional generative neural network [179].

Finally, beyond the linearity in unitary circuits, both deep learning and scalable quantum computation require nonlinearity, to achieve sufficient expressivity for high-level tasks and to realize fundamental units such as CNOT gates, respectively. Recent studies, particularly in deep learning, have focused on separately implementing nonlinearity and unitarity – using photodetection [180], detection-based feedback [76], [77], [181], and all-optical nonlinearity [182], [183]. Considering the advantages of unitary deep learning [46] in mitigating gradient explosion or vanishing problems and the necessity of loss compensation, we can also envisage high-dimensional deep neural networks that preserve unitarity throughout the entire circuit under the concept of nonlinear unitary operations [184].

Author contribution: KK and KP contributed equally to this work. XP and NP supervised the project, mainly focusing on Sections 3 and 4, respectively. KK and KP provided major contributions to Sections 3.2 and 4.2, as well as Sections 3.3 and 4.3. HP contributed to Sections 3.2 and 3.3. SY primarily contributed to Sections 2 and 3.1. All authors have accepted responsibility for the entire content of this manuscript and approved its submission. All authors contributed to the final manuscript.

References

[1] J. J. Sakurai and J. Napolitano, *Modern Quantum Mechanics*, Cambridge, Cambridge University Press, 2020.

[2] M. H. Stone, "On one-parameter unitary groups in Hilbert space," *Ann. Math.*, vol. 33, no. 3, pp. 643−648, 1932.

[3] M. A. Nielsen and I. Chuang, *Quantum Computation and Quantum Information*, Cambridge, Cambridge University Press, 2002.

[4] M. Born and E. Wolf, *Principles of Optics: Electromagnetic Theory of Propagation, Interference and Diffraction of Light*, London, Elsevier, 2013.

[5] M. O. Scully and M. S. Zubairy, *Quantum Optics*, New York, Cambridge University Press, 1997.

[6] S. Longhi, "Quantum-optical analogies using photonic structures," *Laser Photonics Rev.*, vol. 3, no. 3, pp. 243−261, 2009.

[7] D. Dragoman and M. Dragoman, *Quantum-Classical Analogies*, vol. 92, Berlin, Springer, 2004.

[8] A. Aspuru-Guzik and P. Walther, "Photonic quantum simulators," *Nat. Phys.*, vol. 8, no. 4, pp. 285−291, 2012.

[9] A. Yamilov, S. E. Skipetrov, T. W. Hughes, M. Minkov, Z. Yu, and H. Cao, "Anderson localization of electromagnetic waves in three dimensions," *Nat. Phys.*, vol. 19, no. 9, pp. 1308−1313, 2023.

[10] N. C. Harris, *et al.*, "Quantum transport simulations in a programmable nanophotonic processor," *Nat. Photonics*, vol. 11, no. 7, pp. 447−452, 2017.

[11] T. Dai, *et al.*, "A programmable topological photonic chip," *Nat. Mater.*, vol. 23, pp. 928−936, 2024.

[12] M. B. On, F. Ashtiani, D. Sanchez-Jacome, D. Perez-Lopez, S. B. Yoo, and A. Blanco-Redondo, "Programmable integrated photonics for topological Hamiltonians," *Nat. Commun.*, vol. 15, no. 1, p. 629, 2024.

[13] J. Suh, G. Kim, H. Park, S. Fan, N. Park, and S. Yu, "Photonic topological spin pump in synthetic frequency dimensions," *Phys. Rev. Lett.*, vol. 132, no. 3, p. 033803, 2024.

[14] C. Manolatou, M. J. Khan, S. Fan, P. R. Villeneuve, H. A. Haus, and J. D. Joannopoulos, "Coupling of modes analysis of resonant channel add-drop filters," *IEEE J. Quantum Electron.*, vol. 35, no. 9, pp. 1322−1331, 1999.

[15] D. A. Miller, "All linear optical devices are mode converters," *Opt. Express*, vol. 20, no. 21, pp. 23985−23993, 2012.

[16] A. Annoni, *et al.*, "Unscrambling light−automatically undoing strong mixing between modes," *Light Sci. Appl.*, vol. 6, no. 12, p. e17110, 2017.

[17] J. Kim, N. Yu, and Z. Yu, "Compute-first optical detection for noise-resilient visual perception," arXiv preprint arXiv:2403.09612, 2024.

[18] J. D. Joannopoulos, S. G. Johnson, J. N. Winn, and R. D. Meade, *Photonic Crystals: Molding the Flow of Light*, Princeton, Princeton University Press, 2011.

[19] G. Wetzstein, *et al*., "Inference in artificial intelligence with deep optics and photonics," *Nature*, vol. 588, no. 7836, pp. 39−47, 2020.

[20] H. Zhou, *et al*., "Photonic matrix multiplication lights up photonic accelerator and beyond," *Light Sci. Appl.*, vol. 11, no. 1, p. 30, 2022.

[21] C. Huang, *et al*., "Prospects and applications of photonic neural networks," *Adv. Phys. X*, vol. 7, no. 1, p. 1981155, 2022.

[22] A. Tsakyridis, *et al*., "Photonic neural networks and optics-informed deep learning fundamentals," *APL Photonics*, vol. 9, no. 1, 2024. https://doi.org/10.1063/5.0169810.

[23] P. Kok, W. J. Munro, K. Nemoto, T. C. Ralph, J. P. Dowling, and G. J. Milburn, "Linear optical quantum computing with photonic qubits," *Rev. Mod. Phys.*, vol. 79, no. 1, pp. 135−174, 2007.

[24] B. Bartlett and S. Fan, "Universal programmable photonic architecture for quantum information processing," *Phys. Rev. A*, vol. 101, no. 4, p. 042319, 2020.

[25] W. Bogaerts, *et al*., "Programmable photonic circuits," *Nature*, vol. 586, no. 7828, pp. 207−216, 2020.

[26] N. C. Harris, *et al*., "Linear programmable nanophotonic processors," *Optica*, vol. 5, no. 12, pp. 1623−1631, 2018.

[27] A. W. Elshaari, W. Pernice, K. Srinivasan, O. Benson, and V. Zwiller, "Hybrid integrated quantum photonic circuits," *Nat. Photonics*, vol. 14, no. 5, pp. 285−298, 2020.

[28] D. A. Miller, "Perfect optics with imperfect components," *Optica*, vol. 2, no. 8, pp. 747−750, 2015.

[29] W. R. Clements, P. C. Humphreys, B. J. Metcalf, W. S. Kolthammer, and I. A. Walmsley, "Optimal design for universal multiport interferometers," *Optica*, vol. 3, no. 12, pp. 1460−1465, 2016.

[30] M. Y. Saygin, I. Kondratyev, I. Dyakonov, S. Mironov, S. Straupe, and S. Kulik, "Robust architecture for programmable universal unitaries," *Phys. Rev. Lett.*, vol. 124, no. 1, p. 010501, 2020.

[31] M. Moralis-Pegios, G. Giamougiannis, A. Tsakyridis, D. Lazovsky, and N. Pleros, "Perfect linear optics using silicon photonics," *Nat. Commun.*, vol. 15, no. 1, p. 5468, 2024.

[32] R. Tang, R. Tanomura, T. Tanemura, and Y. Nakano, "Ten-port unitary optical processor on a silicon photonic chip," *ACS Photonics*, vol. 8, no. 7, pp. 2074−2080, 2021.

[33] J. R. Rausell-Campo, D. Pérez, and J. C. Francoy, "Programming universal unitary transformations on a general-purpose silicon photonics platform," arXiv preprint arXiv:2407.03235, 2024.

[34] M. Hafezi, E. A. Demler, M. D. Lukin, and J. M. Taylor, "Robust optical delay lines with topological protection," *Nat. Phys.*, vol. 7, no. 11, pp. 907−912, 2011.

[35] S. Jahani and Z. Jacob, "All-dielectric metamaterials," *Nat. Nanotechnol.*, vol. 11, no. 1, pp. 23−36, 2016.

[36] Y. Yang, *et al*., "Programmable high-dimensional Hamiltonian in a photonic waveguide array," *Nat. Commun.*, vol. 15, no. 1, p. 50, 2024.

[37] A. Gonis and W. H. Butler, *Multiple Scattering in Solids*, Berlin, Springer Science & Business Media, 1999.

[38] J. W. Goodman, *Introduction to Fourier Optics*, Greenwood Village, Roberts and Company publishers, 2005.

[39] E. Lustig, Y. Sharabi, and M. Segev, "Topological aspects of photonic time crystals," *Optica*, vol. 5, no. 11, pp. 1390−1395, 2018.

[40] R. Carminati, H. Chen, R. Pierrat, and B. Shapiro, "Universal statistics of waves in a random time-varying medium," *Phys. Rev. Lett.*, vol. 127, no. 9, p. 094101, 2021.

[41] Y. Sharabi, E. Lustig, and M. Segev, "Disordered photonic time crystals," *Phys. Rev. Lett.*, vol. 126, no. 16, p. 163902, 2021.

[42] E. Galiffi, *et al*., "Photonics of time-varying media," *Adv. Photonics*, vol. 4, no. 1, p. 014002, 2022.

[43] J. Kim, D. Lee, S. Yu, and N. Park, "Unidirectional scattering with spatial homogeneity using correlated photonic time disorder," *Nat. Phys.*, vol. 19, no. 5, p. 726, 2023.

[44] R. Tirole, *et al*., "Double-slit time diffraction at optical frequencies," *Nat. Phys.*, vol. 19, no. 7, pp. 999−1002, 2023.

[45] Y. Shen, *et al*., "Deep learning with coherent nanophotonic circuits," *Nat. Photonics*, vol. 11, no. 7, pp. 441−446, 2017.

[46] L. Jing, *et al*., "Tunable efficient unitary neural networks (EUNN) and their application to RNNs," in *International Conference on Machine Learning*, PMLR, 2017, pp. 1733−1741.

[47] E. Khoram, *et al*., "Nanophotonic media for artificial neural inference," *Photonics Res.*, vol. 7, no. 8, pp. 823−827, 2019.

[48] Y. Qu, M. Zhou, E. Khoram, N. Yu, and Z. Yu, "Resonance for analog recurrent neural network," *ACS Photonics*, vol. 9, no. 5, pp. 1647−1654, 2022.

[49] S. Tang, C. Chen, Q. Qin, and X. Liu, "Reconfigurable integrated photonic unitary neural networks with phase encoding enabled by in-situ training," *IEEE Photonics J.*, vol. 16, no. 5, pp. 1−11, 2024.

[50] J. Wang, F. Sciarrino, A. Laing, and M. G. Thompson, "Integrated photonic quantum technologies," *Nat. Photonics*, vol. 14, no. 5, pp. 273−284, 2020.

[51] A. Crespi, *et al*., "Integrated photonic quantum gates for polarization qubits," *Nat. Commun.*, vol. 2, no. 1, p. 566, 2011.

[52] J. Carolan, *et al*., "Universal linear optics," *Science*, vol. 349, no. 6249, pp. 711−716, 2015.

[53] Y. Wang, Z. Hu, B. C. Sanders, and S. Kais, "Qudits and high-dimensional quantum computing," *Front. Phys.*, vol. 8, no. 1, p. 589504, 2020.

[54] Y. Chi, *et al*., "A programmable qudit-based quantum processor," *Nat. Commun.*, vol. 13, no. 1, p. 1166, 2022.

[55] J. Hu, D. Mengu, D. C. Tzarouchis, B. Edwards, N. Engheta, and A. Ozcan, "Diffractive optical computing in free space," *Nat. Commun.*, vol. 15, no. 1, p. 1525, 2024.

[56] O. Kulce, D. Mengu, Y. Rivenson, and A. Ozcan, "All-optical synthesis of an arbitrary linear transformation using diffractive surfaces," *Light Sci. Appl.*, vol. 10, no. 1, p. 196, 2021.

[57] J.-F. Morizur, *et al*., "Programmable unitary spatial mode manipulation," *J. Opt. Soc. Am. A*, vol. 27, no. 11, pp. 2524−2531, 2010.

[58] Y. Wang, V. Potoček, S. M. Barnett, and X. Feng, "Programmable holographic technique for implementing unitary and nonunitary transformations," *Phys. Rev. A*, vol. 95, no. 3, p. 033827, 2017.

[59] C. L. Panuski, *et al*., "A full degree-of-freedom spatiotemporal light modulator," *Nat. Photonics*, vol. 16, no. 12, pp. 834−842, 2022.

[60] R. Yang, *et al*., "Terahertz silicon metagratings: high-efficiency dispersive beam manipulation above diffraction cone," *Laser Photonics Rev.*, vol. 17, no. 7, p. 2200975, 2023.

[61] M. Reck, A. Zeilinger, H. J. Bernstein, and P. Bertani, "Experimental realization of any discrete unitary operator," *Phys. Rev. Lett.*, vol. 73, no. 1, p. 58, 1994.

[62] T. Fu, *et al*., "Photonic machine learning with on-chip diffractive optics," *Nat. Commun.*, vol. 14, no. 1, p. 70, 2023.

[63] A. Haar, "Der Massbegriff in der Theorie der kontinuierlichen Gruppen," *Ann. Math.*, vol. 34, no. 1, pp. 147−169, 1933.

[64] D. Pérez-López, A. M. Gutierrez, E. Sánchez, P. DasMahapatra, and J. Capmany, "Integrated photonic tunable basic units using dual-drive directional couplers," *Opt. Express*, vol. 27, no. 26, pp. 38071−38086, 2019.

[65] P. Orlandi, F. Morichetti, M. J. Strain, M. Sorel, A. Melloni, and P. Bassi, "Tunable silicon photonics directional coupler driven by a transverse temperature gradient," *Opt. Lett.*, vol. 38, no. 6, pp. 863−865, 2013.

[66] A. Sharkawy, S. Shi, D. W. Prather, and R. A. Soref, "Electro-optical switching using coupled photonic crystal waveguides," *Opt. Express*, vol. 10, no. 20, pp. 1048−1059, 2002.

[67] R. Hamerly, S. Bandyopadhyay, and D. Englund, "Asymptotically fault-tolerant programmable photonics," *Nat. Commun.*, vol. 13, no. 1, p. 6831, 2022.

[68] Y. LeCun, L. Bottou, Y. Bengio, and P. Haffner, "Gradient-based learning applied to document recognition," *Proc. IEEE*, vol. 86, no. 11, pp. 2278−2324, 1998.

[69] S. Yu and N. Park, "Heavy tails and pruning in programmable photonic circuits for universal unitaries," *Nat. Commun.*, vol. 14, no. 1, p. 1853, 2023.

[70] Y. Eliezer, U. Rührmair, N. Wisiol, S. Bittner, and H. Cao, "Tunable nonlinear optical mapping in a multiple-scattering cavity," *Proc. Natl. Acad. Sci. U. S. A.*, vol. 120, no. 31, p. e2305027120, 2023.

[71] C. C. Wanjura and F. Marquardt, "Fully nonlinear neuromorphic computing with linear wave scattering," *Nat. Phys.*, vol. 20, no. 9, pp. 1434−1440, 2024.

[72] M. Yildirim, N. U. Dinc, I. Oguz, D. Psaltis, and C. Moser, "Nonlinear processing with linear optics," *Nat. Photonics*, vol. 18, no. 10, pp. 1076−1082, 2024.

[73] H. A. Haus, *Waves and Fields in Optoelectronics*, Englewood Cliffs, Prentice Hall, 1984.

[74] N. C. Harris, *et al*., "Efficient, compact and low loss thermo-optic phase shifter in silicon," *Opt. Express*, vol. 22, no. 9, pp. 10487−10493, 2014.

[75] J. M. Arrazola, *et al*., "Quantum circuits with many photons on a programmable nanophotonic chip," *Nature*, vol. 591, no. 7848, pp. 54−60, 2021.

[76] H. Zhang, *et al*., "An optical neural chip for implementing complex-valued neural network," *Nat. Commun.*, vol. 12, no. 1, p. 457, 2021.

[77] G. Mourgias-Alexandris, *et al*., "Noise-resilient and high-speed deep learning with coherent silicon photonics," *Nat. Commun.*, vol. 13, no. 1, p. 5572, 2022.

[78] C. Wang, *et al*., "Integrated lithium niobate electro-optic modulators operating at CMOS-compatible voltages," *Nature*, vol. 562, no. 7725, pp. 101−104, 2018.

[79] P. I. Sund, *et al*., "High-speed thin-film lithium niobate quantum processor driven by a solid-state quantum emitter," *Sci. Adv.*, vol. 9, no. 19, p. eadg7268, 2023.

[80] M. Dong, *et al*., "High-speed programmable photonic circuits in a cryogenically compatible, visible−near-infrared 200 mm CMOS architecture," *Nat. Photonics*, vol. 16, no. 1, pp. 59−65, 2022.

[81] M. Dong, *et al*., "Synchronous micromechanically resonant programmable photonic circuits," *Nat. Commun.*, vol. 14, no. 1, p. 7716, 2023.

[82] T. W. Hughes, M. Minkov, Y. Shi, and S. Fan, "Training of photonic neural networks through in situ backpropagation and gradient measurement," *Optica*, vol. 5, no. 7, pp. 864−871, 2018.

[83] S. Pai, *et al*., "Experimentally realized in situ backpropagation for deep learning in photonic neural networks," *Science*, vol. 380, no. 6643, pp. 398−404, 2023.

[84] D. A. Miller, "Setting up meshes of interferometers−reversed local light interference method," *Opt. Express*, vol. 25, no. 23, pp. 29233−29248, 2017.

[85] S. Pai, *et al*., "Parallel programming of an arbitrary feedforward photonic network," *IEEE J. Sel. Top. Quantum Electron.*, vol. 26, no. 5, pp. 1−13, 2020.

[86] D. A. Miller, "Self-configuring universal linear optical component," *Photonics Res.*, vol. 1, no. 1, pp. 1−15, 2013.

[87] D. A. Miller, "Self-aligning universal beam coupler," *Opt. Express*, vol. 21, no. 5, pp. 6360−6370, 2013.

[88] S. Pai, B. Bartlett, O. Solgaard, and D. A. Miller, "Matrix optimization on universal unitary photonic devices," *Phys. Rev. Appl.*, vol. 11, no. 6, p. 064044, 2019.

[89] S. Bandyopadhyay, R. Hamerly, and D. Englund, "Hardware error correction for programmable photonics," *Optica*, vol. 8, no. 10, pp. 1247−1255, 2021.

[90] R. Hamerly, S. Bandyopadhyay, and D. Englund, "Stability of self-configuring large multiport interferometers," *Phys. Rev. Appl.*, vol. 18, no. 2, p. 024018, 2022.

[91] R. Hamerly, S. Bandyopadhyay, and D. Englund, "Accurate self-configuration of rectangular multiport interferometers," *Phys. Rev. Appl.*, vol. 18, no. 2, p. 024019, 2022.

[92] R. Burgwal, *et al*., "Using an imperfect photonic network to implement random unitaries," *Opt. Express*, vol. 25, no. 23, pp. 28236−28245, 2017.

[93] A.-L. Barabási, *Network Science*, Cambridge, Cambridge University Press, 2016.

[94] S. Banerjee, M. Nikdast, S. Pasricha, and K. Chakrabarty, "Pruning coherent integrated photonic neural networks," *IEEE J. Sel. Top. Quantum Electron.*, vol. 29, no. 2, pp. 1−13, 2023.

[95] T. Xu, *et al*., "Control-free and efficient integrated photonic neural networks via hardware-aware training and pruning," *Optica*, vol. 11, no. 8, pp. 1039−1049, 2024.

[96] X. Xu, *et al*., "Self-calibrating programmable photonic integrated circuits," *Nat. Photonics*, vol. 16, no. 8, pp. 595−602, 2022.

[97] J. Mower, N. C. Harris, G. R. Steinbrecher, Y. Lahini, and D. Englund, "High-fidelity quantum state evolution in imperfect photonic integrated circuits," *Phys. Rev. A*, vol. 92, no. 3, p. 032322, 2015.

[98] L. Yuan, Y. Shi, and S. Fan, "Photonic gauge potential in a system with a synthetic frequency dimension," *Opt. Lett.*, vol. 41, no. 4, pp. 741−744, 2016.

[99] Q. Lin, M. Xiao, L. Yuan, and S. Fan, "Photonic Weyl point in a two-dimensional resonator lattice with a synthetic frequency dimension," *Nat. Commun.*, vol. 7, no. 1, p. 13731, 2016.

[100] L. Yuan, Q. Lin, M. Xiao, and S. Fan, "Synthetic dimension in photonics," *Optica*, vol. 5, no. 11, pp. 1396−1405, 2018.

[101] A. Dutt, *et al*., "Creating boundaries along a synthetic frequency dimension," *Nat. Commun.*, vol. 13, no. 1, p. 3377, 2022.

[102] D. Cheng, K. Wang, and S. Fan, "Artificial non-Abelian lattice gauge fields for photons in the synthetic frequency dimension," *Phys. Rev. Lett.*, vol. 130, no. 8, p. 083601, 2023.

[103] C. Qin, *et al.*, "Temporal goos-hänchen shift in synthetic discrete-time heterolattices," *Phys. Rev. Lett.*, vol. 133, no. 8, p. 083802, 2024.

[104] C. García-Meca, A. M. Ortiz, and R. L. Sáez, "Supersymmetry in the time domain and its applications in optics," *Nat. Commun.*, vol. 11, no. 1, p. 813, 2020.

[105] X. Wang, M. S. Mirmoosa, V. S. Asadchy, C. Rockstuhl, S. Fan, and S. A. Tretyakov, "Metasurface-based realization of photonic time crystals," *Sci. Adv.*, vol. 9, no. 14, p. eadg7541, 2023.

[106] X. Piao, S. Yu, and N. Park, "Programmable photonic time circuits for highly scalable universal unitaries," *Phys. Rev. Lett.*, vol. 132, no. 10, p. 103801, 2024.

[107] M. Notomi and S. Mitsugi, "Wavelength conversion via dynamic refractive index tuning of a cavity," *Phys. Rev. A*, vol. 73, no. 5, p. 051803, 2006.

[108] Z. Yu and S. Fan, "Complete optical isolation created by indirect interband photonic transitions," *Nat. Photonics*, vol. 3, no. 2, pp. 91−94, 2009.

[109] K. Fang, Z. Yu, and S. Fan, "Realizing effective magnetic field for photons by controlling the phase of dynamic modulation," *Nat. Photonics*, vol. 6, no. 11, pp. 782−787, 2012.

[110] J. Park, *et al.*, "Revealing non-Hermitian band structure of photonic Floquet media," *Sci. Adv.*, vol. 8, no. 40, p. eabo6220, 2022.

[111] M. Hafezi, S. Mittal, J. Fan, A. Migdall, and J. M. Taylor, "Imaging topological edge states in silicon photonics," *Nat. Photonics*, vol. 7, no. 12, pp. 1001−1005, 2013.

[112] T. Ozawa, *et al.*, "Topological photonics," *Rev. Mod. Phys.*, vol. 91, no. 1, p. 015006, 2019.

[113] H. Park, X. Piao, and S. Yu, "Scalable and programmable emulation of photonic hyperbolic lattices," *ACS Photonics*, vol. 11, no. 9, pp. 3890−3897, 2024.

[114] G. Kim, J. Li, X. Piao, N. Park, and S. Yu, "Programmable lattices for non-Abelian topological photonics and braiding," arXiv preprint arXiv:2410.01181, 2024.

[115] J. G. Proakis and D. K. Manolakis, *Digital Signal Processing: Principles, Algorithms, and Applications, 4/E*, London, Prentice-Hall, 2006.

[116] F. Zangeneh-Nejad, D. L. Sounas, A. Alù, and R. Fleury, "Analogue computing with metamaterials," *Nat. Rev. Mater.*, vol. 6, no. 3, pp. 207−225, 2021.

[117] M. Miscuglio, *et al.*, "Approximate analog computing with metatronic circuits," *Commun. Phys.*, vol. 4, no. 1, p. 196, 2021.

[118] H. Goh and A. Alù, "Nonlocal scatterer for compact wave-based analog computing," *Phys. Rev. Lett.*, vol. 128, no. 7, p. 073201, 2022.

[119] A. Silva, F. Monticone, G. Castaldi, V. Galdi, A. Alù, and N. Engheta, "Performing mathematical operations with metamaterials," *Science*, vol. 343, no. 6167, pp. 160−163, 2014.

[120] S. K. Vadlamani, D. Englund, and R. Hamerly, "Transferable learning on analog hardware," *Sci. Adv.*, vol. 9, no. 28, p. eadh3436, 2023.

[121] M. W. Puckett, *et al.*, "422 Million intrinsic quality factor planar integrated all-waveguide resonator with sub-MHz linewidth," *Nat. Commun.*, vol. 12, no. 1, p. 934, 2021.

[122] Y. Tanaka, J. Upham, T. Nagashima, T. Sugiya, T. Asano, and S. Noda, "Dynamic control of the Q factor in a photonic crystal nanocavity," *Nat. Mater.*, vol. 6, no. 11, pp. 862−865, 2007.

[123] V. Namias, "The fractional order Fourier transform and its application to quantum mechanics," *IMA J. Appl. Math.*, vol. 25, no. 3, pp. 241−265, 1980.

[124] S. Weimann, *et al.*, "Implementation of quantum and classical discrete fractional Fourier transforms," *Nat. Commun.*, vol. 7, no. 1, p. 11027, 2016.

[125] M. Markowitz, K. Zelaya, and M.-A. Miri, "Learning arbitrary complex matrices by interlacing amplitude and phase masks with fixed unitary operations," *Phys. Rev. A*, vol. 110, no. 3, p. 033501, 2024.

[126] G. Nienhuis and L. Allen, "Paraxial wave optics and harmonic oscillators," *Phys. Rev. A*, vol. 48, no. 1, p. 656, 1993.

[127] S. Yu, X. Piao, and N. Park, "Controlling random waves with digital building blocks based on supersymmetry," *Phys. Rev. Appl.*, vol. 8, no. 5, p. 054010, 2017.

[128] R. G. Dorsch, A. W. Lohmann, Y. Bitran, D. Mendlovic, and H. M. Ozaktas, "Chirp filtering in the fractional Fourier domain," *Appl. Opt.*, vol. 33, no. 32, pp. 7599−7602, 1994.

[129] N. M. Atakishiyev and K. B. Wolf, "Fractional Fourier−Kravchuk transform," *J. Opt. Soc. Am. A*, vol. 14, no. 7, pp. 1467−1477, 1997.

[130] R. Gordon, "Harmonic oscillation in a spatially finite array waveguide," *Opt. Lett.*, vol. 29, no. 23, pp. 2752−2754, 2004.

[131] L. Verslegers, P. B. Catrysse, Z. Yu, and S. Fan, "Deep-subwavelength focusing and steering of light in an aperiodic metallic waveguide array," *Phys. Rev. Lett.*, vol. 103, no. 3, p. 033902, 2009.

[132] D. N. Christodoulides, F. Lederer, and Y. Silberberg, "Discretizing light behaviour in linear and nonlinear waveguide lattices," *Nature*, vol. 424, no. 6950, pp. 817−823, 2003.

[133] M. Markowitz, K. Zelaya, and M.-A. Miri, "Auto-calibrating universal programmable photonic circuits: hardware error-correction and defect resilience," *Opt. Express*, vol. 31, no. 23, pp. 37673−37682, 2023.

[134] K. Zelaya, M. Markowitz, and M.-A. Miri, "The Goldilocks principle of learning unitaries by interlacing fixed operators with programmable phase shifters on a photonic chip," *Sci. Rep.*, vol. 14, no. 1, p. 10950, 2024.

[135] K. Zelaya and M.-A. Miri, "Integrated photonic fractional convolution accelerator," *Photonics Res.*, vol. 12, no. 8, pp. 1828−1839, 2024.

[136] K. Levenberg, "A method for the solution of certain non-linear problems in least squares," *Q. Appl. Math.*, vol. 2, no. 2, pp. 164−168, 1944.

[137] D. W. Marquardt, "An algorithm for least-squares estimation of nonlinear parameters," *J. Soc. Ind. Appl. Math.*, vol. 11, no. 2, pp. 431−441, 1963.

[138] R. M. Gray, "Toeplitz and circulant matrices: a review," *Found. Trends Commun. Inf. Theory*, vol. 2, no. 3, pp. 155−239, 2006.

[139] M. Huhtanen and A. Perämäki, "Factoring matrices into the product of circulant and diagonal matrices," *J. Fourier Anal. Appl.*, vol. 21, no. 5, pp. 1018−1033, 2015.

[140] K. Zelaya and M.-A. Miri, "Photonic matrix multiplier makes a direction-finding sensor," arXiv preprint arXiv:2411.06731, 2024.

[141] B. Niewelt, *et al.*, "Experimental implementation of the optical fractional Fourier transform in the time-frequency domain," *Phys. Rev. Lett.*, vol. 130, no. 24, p. 240801, 2023.

[142] T. Ozawa, H. M. Price, N. Goldman, O. Zilberberg, and I. Carusotto, "Synthetic dimensions in integrated photonics: from

optical isolation to four-dimensional quantum Hall physics," *Phys. Rev. A*, vol. 93, no. 4, p. 043827, 2016.

[143] L. Yuan, M. Xiao, Q. Lin, and S. Fan, "Synthetic space with arbitrary dimensions in a few rings undergoing dynamic modulation," *Phys. Rev. B*, vol. 97, no. 10, p. 104105, 2018.

[144] L. Yuan and S. Fan, "Bloch oscillation and unidirectional translation of frequency in a dynamically modulated ring resonator," *Optica*, vol. 3, no. 9, pp. 1014−1018, 2016.

[145] J. Park, *et al*., "Spontaneous emission decay and excitation in photonic temporal crystals," arXiv preprint arXiv:2404.13287, 2024.

[146] A. Dutt, M. Minkov, Q. Lin, L. Yuan, D. A. Miller, and S. Fan, "Experimental band structure spectroscopy along a synthetic dimension," *Nat. Commun.*, vol. 10, no. 1, p. 3122, 2019.

[147] S. Buddhiraju, A. Dutt, M. Minkov, I. A. Williamson, and S. Fan, "Arbitrary linear transformations for photons in the frequency synthetic dimension," *Nat. Commun.*, vol. 12, no. 1, p. 2401, 2021.

[148] G. Kim, J. Suh, D. Lee, N. Park, and S. Yu, "Long-range-interacting topological photonic lattices breaking channel-bandwidth limit," *Light Sci. Appl.*, vol. 13, no. 1, p. 189, 2024.

[149] R. H. Byrd, P. Lu, J. Nocedal, and C. Zhu, "A limited memory algorithm for bound constrained optimization," *SIAM J. Sci. Comput.*, vol. 16, no. 5, pp. 1190−1208, 1995.

[150] K. Fang, Z. Yu, and S. Fan, "Photonic Aharonov−Bohm effect based on dynamic modulation," *Phys. Rev. Lett.*, vol. 108, no. 15, p. 153901, 2012.

[151] N. Tischler, C. Rockstuhl, and K. Słowik, "Quantum optical realization of arbitrary linear transformations allowing for loss and gain," *Phys. Rev. X*, vol. 8, no. 2, p. 021017, 2018.

[152] X. Ji, *et al*., "On-chip tunable photonic delay line," *APL Photonics*, vol. 4, no. 9, 2019. https://doi.org/10.1063/1.5111164.

[153] T. Yan, *et al*., "Fourier-space diffractive deep neural network," *Phys. Rev. Lett.*, vol. 123, no. 2, p. 023901, 2019.

[154] Y. Li, I. Liberal, C. Della Giovampaola, and N. Engheta, "Waveguide metatronics: lumped circuitry based on structural dispersion," *Sci. Adv.*, vol. 2, no. 6, p. e1501790, 2016.

[155] S. Yu, "Evolving scattering networks for engineering disorder," *Nat. Comput. Sci.*, vol. 3, no. 2, pp. 128−138, 2023.

[156] S. Yu, C.-W. Qiu, Y. Chong, S. Torquato, and N. Park, "Engineered disorder in photonics," *Nat. Rev. Mater.*, vol. 6, no. 3, pp. 226−243, 2021.

[157] C. Guo and S. Fan, "Unitary control of partially coherent waves. I. Absorption," *Phys. Rev. B*, vol. 110, no. 3, p. 035430, 2024.

[158] C. Guo and S. Fan, "Unitary control of partially coherent waves. II. Transmission or reflection," *Phys. Rev. B*, vol. 110, no. 3, p. 035431, 2024.

[159] C. Guo, D. A. Miller, and S. Fan, "Unitary control of multiport wave transmission," arXiv preprint arXiv:2408.05634, 2024.

[160] C. Roques-Carmes, S. Fan, and D. A. Miller, "Measuring, processing, and generating partially coherent light with self-configuring optics," *Light Sci. Appl.*, vol. 13, no. 1, p. 260, 2024.

[161] S. Yu, X. Piao, and N. Park, "Neuromorphic functions of light in parity-time-symmetric systems," *Adv. Sci.*, vol. 6, no. 15, p. 1900771, 2019.

[162] S. Yu, X. Piao, and N. Park, "Topologically protected optical signal processing using parity-time-symmetric oscillation quenching," *Nanophotonics*, vol. 10, no. 11, pp. 2883−2891, 2021.

[163] S. Choi, J. Kim, J. Kwak, N. Park, and S. Yu, "Topologically protected all-optical memory," *Adv. Electron. Mater.*, vol. 8, no. 10, p. 2200579, 2022.

[164] A. Suntharalingam, L. Fernández-Alcázar, R. Kononchuk, and T. Kottos, "Noise resilient exceptional-point voltmeters enabled by oscillation quenching phenomena," *Nat. Commun.*, vol. 14, no. 1, p. 5515, 2023.

[165] K. Wang, A. Dutt, C. C. Wojcik, and S. Fan, "Topological complex-energy braiding of non-Hermitian bands," *Nature*, vol. 598, no. 7879, pp. 59−64, 2021.

[166] C. Nayak, S. H. Simon, A. Stern, M. Freedman, and S. D. Sarma, "Non-Abelian anyons and topological quantum computation," *Rev. Mod. Phys.*, vol. 80, no. 3, pp. 1083−1159, 2008.

[167] A. Mirhoseini, *et al*., "A graph placement methodology for fast chip design," *Nature*, vol. 594, no. 7862, pp. 207−212, 2021.

[168] O. Lib and Y. Bromberg, "Quantum light in complex media and its applications," *Nat. Phys.*, vol. 18, no. 9, pp. 986−993, 2022.

[169] W. Ma, Z. Liu, Z. A. Kudyshev, A. Boltasseva, W. Cai, and Y. Liu, "Deep learning for the design of photonic structures," *Nat. Photonics*, vol. 15, no. 2, pp. 77−90, 2021.

[170] R. S. Hegde, "Deep learning: a new tool for photonic nanostructure design," *Nanoscale Adv.*, vol. 2, no. 3, pp. 1007−1023, 2020.

[171] D. Liu, Y. Tan, E. Khoram, and Z. Yu, "Training deep neural networks for the inverse design of nanophotonic structures," *ACS Photonics*, vol. 5, no. 4, pp. 1365−1369, 2018.

[172] S. Yu, X. Piao, and N. Park, "Machine learning identifies scale-free properties in disordered materials," *Nat. Commun.*, vol. 11, no. 1, p. 4842, 2020.

[173] P. R. Wiecha, A. Arbouet, C. Girard, and O. L. Muskens, "Deep learning in nano-photonics: inverse design and beyond," *Photonics Res.*, vol. 9, no. 5, pp. B182−B200, 2021.

[174] K. O. Stanley, J. Clune, J. Lehman, and R. Miikkulainen, "Designing neural networks through neuroevolution," *Nat. Mach. Intell.*, vol. 1, no. 1, pp. 24−35, 2019.

[175] S. Whitelam, V. Selin, S.-W. Park, and I. Tamblyn, "Correspondence between neuroevolution and gradient descent," *Nat. Commun.*, vol. 12, no. 1, p. 6317, 2021.

[176] J. Kennedy and R. Eberhart, "Particle swarm optimization," in *Proceedings of ICNN'95-International Conference on Neural Networks*, vol. 4, IEEE, 1995, pp. 1942−1948.

[177] J. Kim, Q. Zhou, and Z. Yu, "Photonic systolic array for all-optical matrix-matrix multiplication," arXiv preprint arXiv:2410.21671, 2024.

[178] M. Zhou, *et al*., "Inverse design of metasurfaces based on coupled-mode theory and adjoint optimization," *ACS Photonics*, vol. 8, no. 8, pp. 2265−2273, 2021.

[179] J. Jiang and J. A. Fan, "Global optimization of dielectric metasurfaces using a physics-driven neural network," *Nano Lett.*, vol. 19, no. 8, pp. 5366−5372, 2019.

[180] X. Lin, *et al*., "All-optical machine learning using diffractive deep neural networks," *Science*, vol. 361, no. 6406, pp. 1004−1008, 2018.

[181] A. N. Tait, *et al*., "Neuromorphic photonic networks using silicon photonic weight banks," *Sci. Rep.*, vol. 7, no. 1, p. 7430, 2017.

[182] G. Mourgias-Alexandris, A. Tsakyridis, N. Passalis, A. Tefas, K. Vyrsokinos, and N. Pleros, "An all-optical neuron with sigmoid activation function," *Opt. Express*, vol. 27, no. 7, pp. 9620−9630, 2019.

[183] Y. Zuo, *et al*., "All-optical neural network with nonlinear activation functions," *Optica*, vol. 6, no. 9, pp. 1132−1137, 2019.

[184] S. Yu, X. Piao, and N. Park, "Nonlinear unitary circuits for photonic neural networks," arXiv preprint arXiv:2412.04112, 2024.